Spring 5-5-2023

Investigation of Spatial Frequency Domain Imaging Analysis in Diabetic Foot Testing and Microneedle Treatments

Christian Crane
University of Maine, christian.crane@maine.edu

Investigation of Spatial Frequency Domain Imaging Analysis in Diabetic Foot Testing and Microneedle Treatments

By

Christian Crane

A Thesis

Submitted in Partial Fulfillment of the

Requirements for the Degree of

Master of Science

(in Biomedical Engineering)

The Graduate School

The University of Maine

May 2023

Advisory Committee

Karissa Tilbury, Ph.D. Biomedical Engineering - Advisor, Chair

Robert Bowie, M.D. Medicine and Surgery - Member

Michael Mason, Ph.D. Chemistry - Member

Investigation of Spatial Frequency Domain Imaging Analysis in Diabetic Foot Testing and Microneedle Treatments

By Christian Crane

Thesis Advisor: Dr. Karissa Tilbury

An Abstract of the Thesis Presented
in Partial Fulfillment of the Requirements for the
Degree of Master of Science
(in Biomedical Engineering)
May 2023

Spatial Frequency Domain Imaging (SFDI) is a wide-field optical technique that utilizes spatially modulated selective wavelengths of light to probe biological tissue. Diffuse reflected light from the sample is compared to a table of values, extracted from a photon propagation simulation, to correlate experimental data to optical properties (absorption, scattering). The decoupling of absorption from scattering across multiple wavelengths allows for quantified chromophore content estimation within tissue. Biological chromophores are often associated with physiologic mechanisms and are key to quantifying disease progression.

Exploration and verification of novel clinical utility of SFDI is essential for the potential benefit to medical outcomes of a variety of disease states and for adoption of the technology. In this work, the chromophore hemoglobin is used as a key metric for perfusion quality including total blood content in a region of interest and oxygen saturation. We aimed to test this technique in two new applications to add to the growing list of clinical research. Presented in this paper is a brief overview of SFDI, perfusion reactivity analysis of microneedle treatment, and a pilot study utilizing SFDI to analyze diabetic and neuropathic feet in several postural positions. Results from each previously mentioned use case indicate potential sensitivity to physiologic mechanisms such as pressure induced vasodilation, blood pooling, and vascular dysregulation. Additional research into postural regulation effects on perfusion of the diabetic foot is recommended as this pilot study indicated potential for neuropathic damage detection through perfusion metrics.

Acknowledgements

I would like to thank my graduate advisor and chair of my committee for her patience and guidance during my graduate career. I also want to acknowledge my thesis committee for their knowledge and assistance. In addition to these professional associations, I would like to acknowledge the students within the Tilbury lab as they have been wonderful to work alongside and learn from.

A further gratitude for my family, friends, and college acquaintances who found interest in my research and aided in keeping my motivation high. Many of these people also were so kind to participate in my research directly, which I thoroughly appreciate.

Finally, I'd like to thank the University of Maine Center for Undergraduate Research for partial funding of this research.

TABLE OF CONTENTS

LIST OF TABLES

LIST OF FIGURES

LIST OF EQUATIONS

CHAPTER 1

Spatial Frequency Domain Imaging Background and Principles

The following chapter is organized as an introduction into SFDI considering, the process of hardware selection, data acquisition, analysis steps in detail, and relevant data output.

Background

Optical imaging techniques are important in medicine already comprising 64% of all medical imaging expenditures globally.[1] Optical systems mitigate radiation exposure. Spatial Frequency domain imaging (SFDI) is an optical technique with ~ 1 mm resolution used to quantify physiological tissue parameters such as tissue perfusion via oxy- and deoxyhemoglobin with no hazardous radiation. SFDI uses spatially projected patterns enabling the extraction of absorption and scattering coefficients within sampled tissue volumes. These optical coefficients are then correlated with chromophore concentrations (absorption) or structural changes (scattering) within the sampled tissue to give valuable physiologic information. Quantified tissue chromophore values from SFDI have proven useful for many medical applications including burn severity classification,[2,3] vascular assessment,[4,5,6] and surgical guidance[7,8]. In the following chapters we will explore the basic principles of SFDI and two applications for SFDI: microneedle treatment analysis and diabetic perfusion quantification.

Overview

Spatial frequency domain imaging relies on the detection of variation in the modulation transfer function incurred by the sample. The use of spatial projections allows for selectivity in average photon depth where increasing spatial frequency decreases average photon depth in tissue.[9] This in combination with selected wavelengths allow for combinations of system specifications to increase accuracy for desired goals such as the use of short wavelengths of visible light in conjunction with higher spatial frequencies (0.2/mm) for superficial tissue quantification targeting melanin concentration. SFDI techniques allow for many potential medical applications to be studied at a low-cost.

An overview of SFDI data collection and analysis is provided below (Fig. 1) is taken from the 2019 SFDI review article.[10] To begin data collection a light source (LED or LASER) creates a desired wavelength of light which interfaces with a patterning device (DMD or projector). This projected DC or AC (spatial frequency) pattern of photons diffuses into the tissue then returns to the associated camera for detection. The detected raw values are

demodulated (Fig. 2) and calibrated (Eq. 1) relative to a tissue mimicking phantom with known optical properties. Demodulating and calibrating the collected values returns the tissue response as deviation from the projected pattern alongside diffuse reflectance of the sample. This variation of light is the modulation transfer function imparted onto the projection by the tissue sample (S-MTF). Then the estimated diffuse reflectance at two spatial frequency points is compared to pre-simulated look-up tables (LUT) to estimate absorption and scattering coefficients. Finally, the estimated absorption at each desired wavelength is used with the inverse Beer-Lambert law (Eq. 4) to approximate chromophore concentrations. These chromophore concentrations may then be correlated to disease tissue or reported back to clinicians as a diagnostic tool.

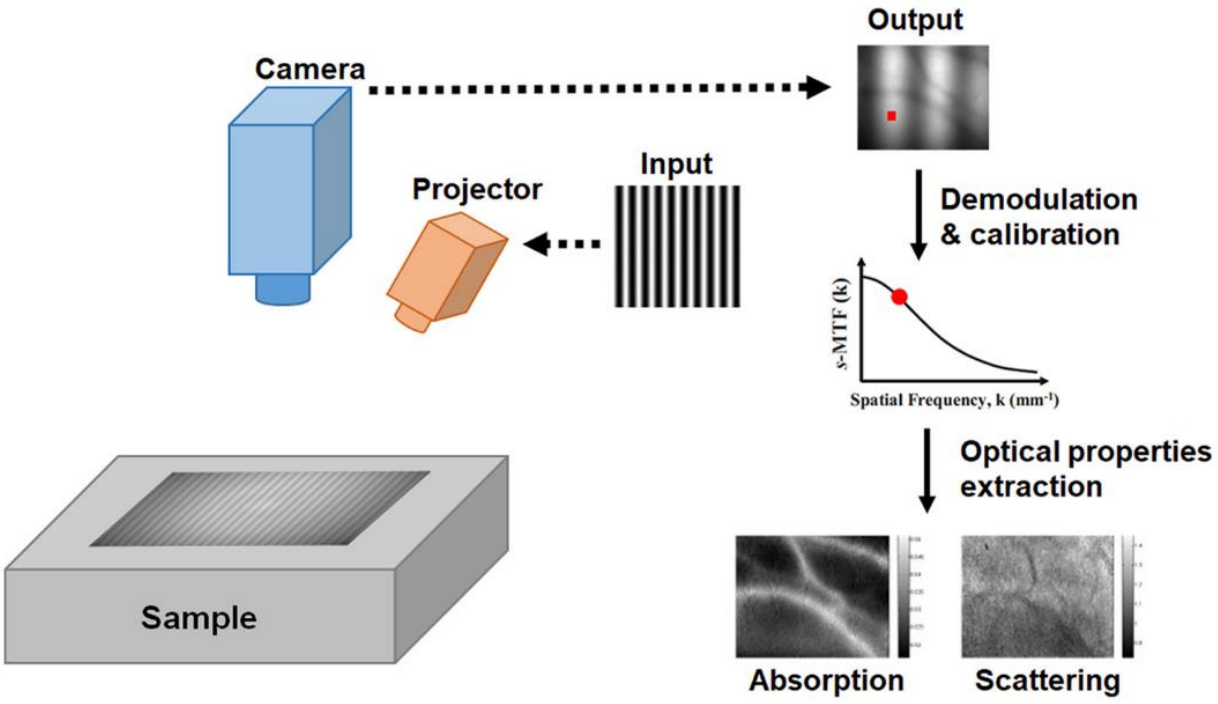

Figure 1: SFDI system data collection and analysis pathway overview. Adapted from Ref. 1.

Hardware Considerations

Wavelength Selection. SFDI uses wavelengths of light in the visible (400-650 nm), near-infrared (650-1000nm) and short-wave infrared (SWIR 1000-2500nm). The wavelength of light used is dependent in part on both the penetration depth and the tissue chromophores to be quantified. Sampling depth in SFDI is correlated with the spatial frequency of projected light, wavelength of light, and optically active tissue absorbers and scattering structures. Increasing spatial frequency reduces sampling depth due to turbid media acting as a low-pass filter.[11] Sampling depth varies across sample types due to chromophore absorption and scattering spectra which depends on

the physiological region being sampled. For example, skin has lower penetration in the NIR region than brain or breast tissue.[12]

Some of the commonly quantified chromophores are oxyhemoglobin (HbO2), deoxyhemoglobin (HHb), lipids, water, and melanin. Each of these chromophores have known absorption spectra over a wide range of wavelengths. Selecting the desired wavelengths to match with substantial changes in chromophore absorption spectra allows for extraction of concentration within tissue which will be discussed later in this chapter. Wavelengths between 650-1000nm are often selected to distinguish HbO2 and HHb due to an inversion in absorption called an isosbestic point. This allows a linear combination of the two chromophores to estimate concentration.[12]

Light emitting diodes (LED) and light amplification by stimulated emission of radiation (LASER) are the two most common SFDI light sources. Generally, the benefit of coherence that LASER systems provide is mitigated due to the diffuse nature of tissue samples. However, the tunability and collimating properties of some LASER light does mitigate the need for other hardware such as multiple LEDs for multiple wavelengths or collimating lens.

Digital Micromirror Device / Projector. To project the spatially modulated light onto a sample surface there must be a component to create the pattern of designated spatial frequency. Two commonly used methods are digital light projectors (DLP) and digital micromirror devices (DMD). DLP's have two primary downsides relative to DMDs, increased cost and limited use to three wavelengths. This results in DMD systems to be more versatile allowing a wide spectrum of wavelengths custom chosen for the diffuse imaging system.[13] Following the collimation of light (if using LEDs) it reflects off a programmed DMD which creates spatial frequency patterns, depending on the projection scheme wanted, several phases of the pattern may also be created by this DMD.

Camera. SFDI relies on accurate photon counts reflecting from the sample surface, as such the quality and specification of the camera is highly valuable. Detected photons of background noise and unwanted light collection will be accounted for during the processing calibration step. However, the calibration step relies on the instrument response function (IRF) to remain constant between the calibration data set collection and every sample collection. Sensitivity to unwanted external variables such as unused wavelengths of light may cause data error. Camera spectral sensitivity must be considered to maintain high sensitivity to the spectrum of light used for data collection.

Data Processing

Demodulation

Following image collection, spatial frequency images at three phases 0, 120, 240 degrees are converted into a single image. Single pixel and single snapshot (multipixel) demodulation are two common methods for accomplishing this step. Single pixel is known for the benefit of higher image quality and resolution but requiring rapid sequential image collections. Single snapshot (multipixel) has the benefit of reduced data collection but at the cost of image quality relative to single pixel.

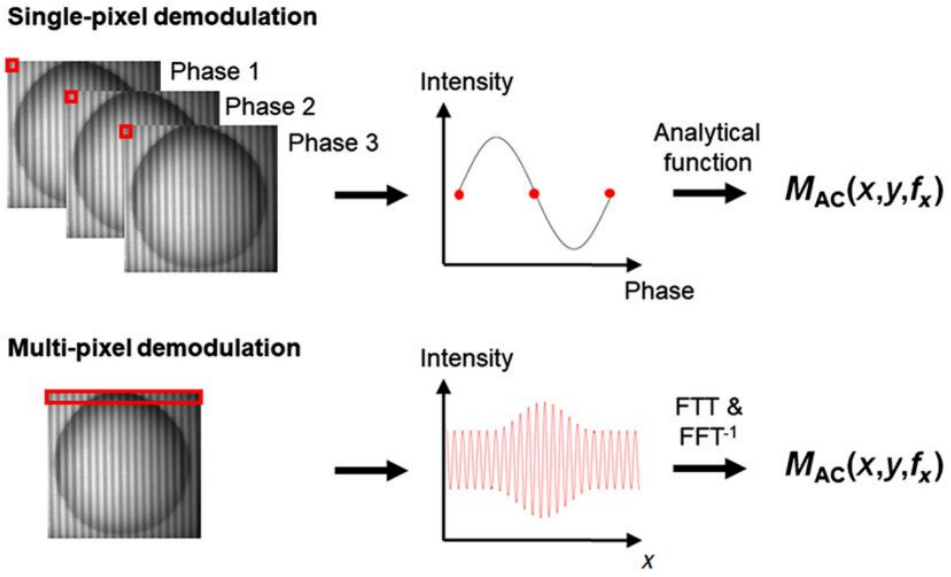

Figure 2: Demodulation techniques: Single and Multi-pixel demodulation where single-pixel demodulation relies on three phase shifted frames and the analytical formula presented in Fig. 3. Multi-pixel relies on a Fourier transform of a row of pixels to extract amplitude modulation.

During this research single pixel, three phase demodulation is used and an example of its process is shown in (Fig. 3). Each pixel at a given spatial frequency and wavelength goes through the shown equation to find the M_{AC} or amplitude modulation of the sample. If the resultant combined image has remaining phase lines an error in hardware or deviation during data collection likely occurred.

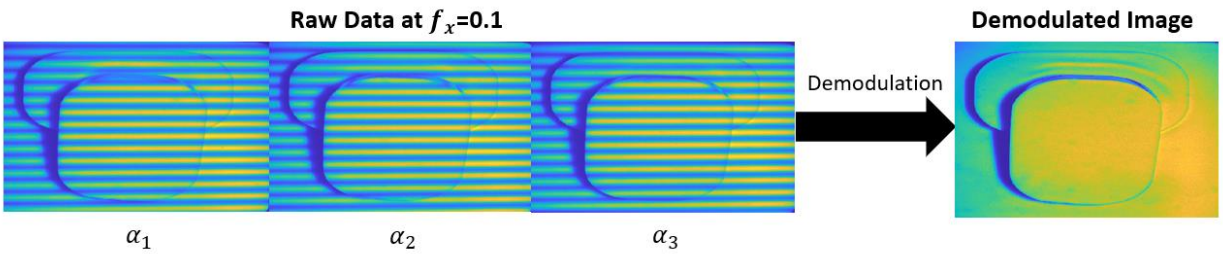

$$M_{AC}(x, f_x) = \frac{\sqrt{2}}{3} * \sqrt{\{[I(x, f_x, \alpha_1) - I(x, f_x, \alpha_2)]^2 + [I(x, f_x, \alpha_2) - I(x, f_x, \alpha_3)]^2 + [I(x, f_x, \alpha_3) - I(x, f_x, \alpha_1)]^2\}}$$

Figure 3: Example of single pixel demodulation at three phases and the output from the presented equation for amplitude modulation.

Calibration

Calibration is the mathematical step in which the instrument response function (IRF) is removed from a data set. To find the IRF, a dataset of equal wavelength and spatial frequency is collected on a sample of a tissue-mimicking reference phantom with known optical properties. It is important that the lighting environment remains stable between phantom data collection and sample collection, or ambient noise will not be accounted for during calibration. The reference dataset is then demodulated giving the resultant reference phantom amplitude modulation $M_{AC,ref}$. Phantom amplitude modulation alongside illumination intensity and a photon propagation model of the reference phantom optical properties approximates the modulation transfer function of the system MTF_{SYS}. In the spatial frequency domain, a simple division of the sample amplitude modulation $M_{AC,sample}$ by the reference phantom amplitude modulation $M_{AC,ref}$ multiplied by predicted diffuse reflectance $R_{d,ref.model}$ yields sample diffuse reflectance (Eq. 1).

Model Inversion (Look Up Table)

Monte Carlo Simulation. To extract optical properties with SFDI a simulation must be completed relating diffuse reflectance at two spatial frequencies to a simulated optical property set. These simulations are completed using a technique called "Monte Carlo" modeling of a diffuse medium. In this simulation photons are sent into a medium of designated absorption, scattering, anisotropy, and reflective index values relevant to biological tissue. The resulting light reflected from the simulated medium allows the calculation of diffuse reflectance as shown in Eq. 1. Where $M_{AC,sample}$ is the modulation in the sample data, $M_{AC,ref}$ is the modulated value of the known optical property data, and $R_{d,ref.model}$ is the corresponding diffuse reflectance for the known optical properties of the phantom.

This relationship between diffuse reflectance and optical properties is how we calculate absorption and scattering coefficients for sample tissues.

$$R_{d,sample} = \frac{M_{AC,sample}}{M_{AC,ref}} * R_{d,ref.model} \quad (1)$$

Optical Property Estimation. Following calibration, diffuse reflectance of the sample at two spatial frequencies and wavelength is searched in a pre-simulated data table (Fig. 4 & 5). Inputting $R_{d,sample}$ at two spatial frequencies into a five-dimensional data cube ($R_{d,AC}, R_{d,DC}, f_x, \mu_a, \mu_s'$) finds an intersection point yielding predicted absorption and scattering coefficients. This is then repeated at every wavelength within the sample dataset resulting in absorption and scattering coefficients for a wavelength spectrum which will be used in chromophore estimation.

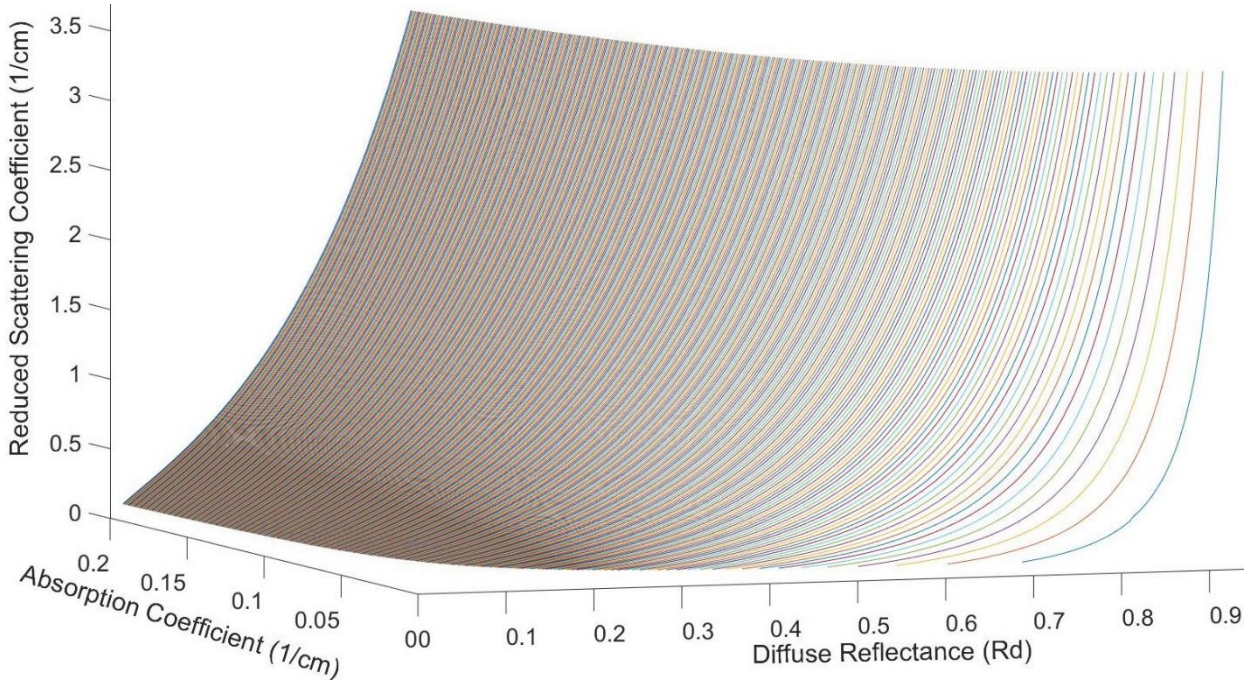

Figure 4: Planar (fx=0/mm) Look Up Table

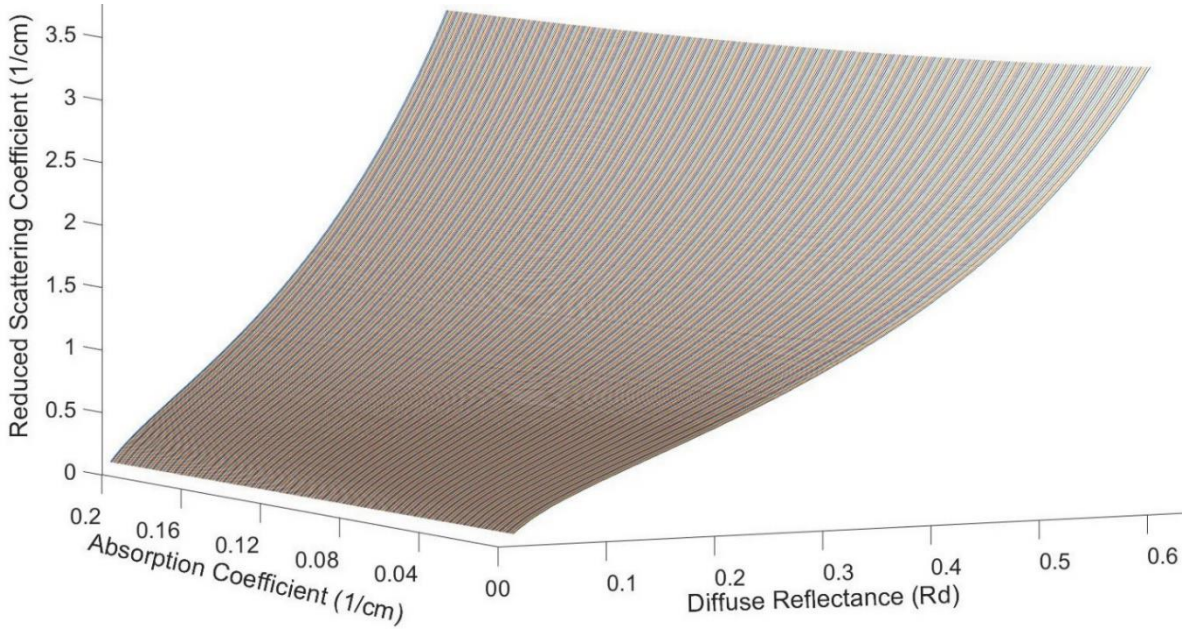

Figure 5: AC signal (fx=0.1/mm) Look Up Table

Chromophore Fitting. The Beer-Lambert law is the overarching principle behind chromophore concentration estimates during SFDI analysis. This law relates absorbance of a sample to transmittance and further elaborates to comparing absorbance with molar extinction coefficients, molar concentration values, and optical path length. An example of varied absorbance can be seen below (Fig. 6) measured through a cuvette of known optical path length (width of cuvette). This correlation between molar extinction coefficients, molar concentration values and absorbance allows for solving the inverse problem to estimate molar concentration values from absorption.

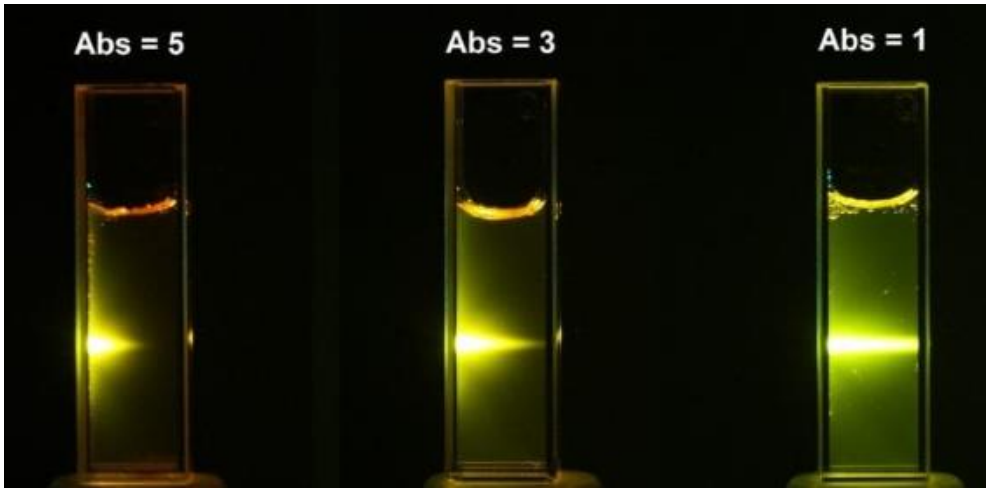

Figure 6: Three cuvettes with differing absorption values seen with fluorescence emission. Adapted from: https://www.edinst.com/blog/the-beer-lambert-law/

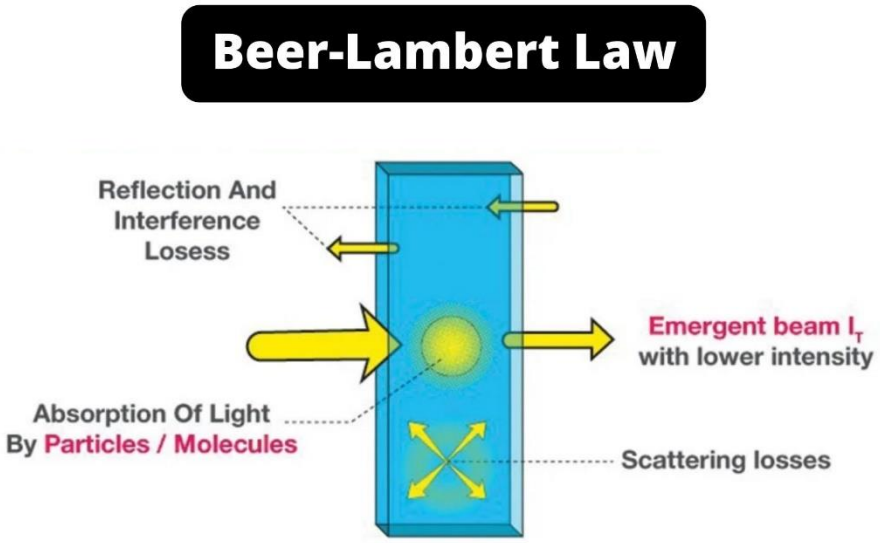

Figure 7: Examples of optical interactions influencing emergent beam intensity. Adapted from https://microbiologynote.com/beer-lambert-law/.

One limitation for the Beer-Lambert law is its ability to estimate values in highly scattering regimes due to inference with the observed absorption. (Fig. 7) Therefore, scattering effects must be separated from sample data to isolate absorption coefficients for use in the inverse Beer-Lambert law. In addition to scattering effects background noise and reflection elements are accounted for using a calibrating optical phantom which allows isolation of the absorption of light. Following estimation of absorption and scattering coefficients the Beer-Lambert law may be used with known extinction coefficients of chromophores to calculate concentration as shown in Eq. 3. Where μ_a is the absorption coefficient for a specific chromophore, C is the molar concentration of chromophore, and ε is the known molar extinction coefficient for the designated chromophore. Using multiple sampled wavelengths in a linear combination, tissue molar chromophore concentrations can be estimated to identify oxy/deoxy-hemoglobin, lipids, water, and melanin. As previously mentioned, the wavelength selection for SFDI analysis is very important to maximize accuracy of chromophore estimates. These two wavelengths are selected to maximize the difference in absorption coefficient between oxy-hemoglobin and deoxy-hemoglobin. This relies on the concept of an isosbestic point which is a specific wavelength where absorbance of multiple substances crosses over to invert the previous relationship. In this case at the lower 650nm wavelength deoxygenated hemoglobin has a higher extinction

coefficient and by extension a higher absorption. Following the isosbestic point at 800nm, oxygenated hemoglobin has a higher absorption at 850nm. (Fig. 8)

$$\mu_a(\lambda) = \ln(10) * \sum \varepsilon(\lambda) * C \quad (2)$$

$$C = \frac{\mu_a(\lambda)}{\ln(10) * \sum \varepsilon(\lambda)} \quad (3)$$

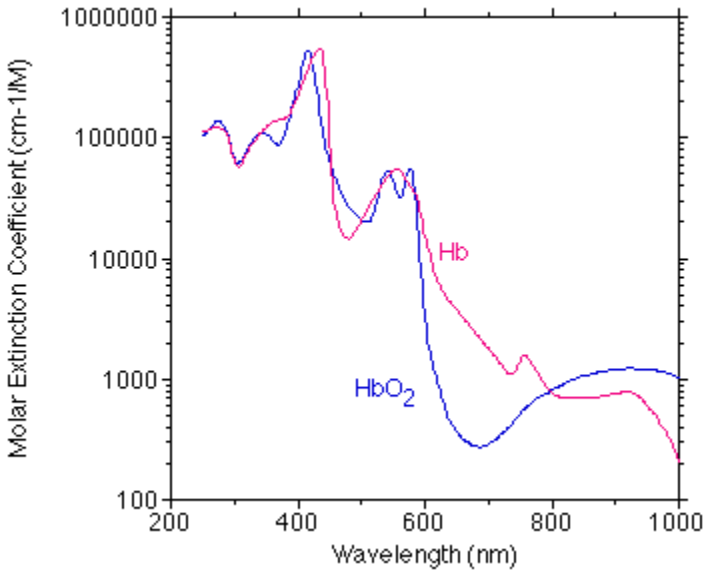

Figure 8: Oxy/Deoxy-Hemoglobin extinction spectra. Adapted from Ref. 18.

Data Error

When using SFDI as a technique it is important to be aware of potential sources of error and the potential impact on chromophore concentration estimates. SFDI requires many baseline assumptions for both look up table generation and data collection. In this section we will review an excellent publication on error in SFDI techniques.[14]

Look Up Table Generation Error

During creation of look up tables (LUT) using Monte-Carlo simulation many variables must be defined with impactful assumptions. Inputs into Monte-Carlo simulations are absorption coefficient, scattering coefficient, anisotropy, and refractive index. Anisotropy describes the asymmetry in the scattering phase function during photon interaction and direction that photon may continue in. A widely used value for anisotropy for biological tissue is 0.9 which indicates a largely forward directionality during scattering events.[2,3,15,16] Incorrect values of anisotropy in simulation may lead to substantial error in reduced scattering and absorption coefficients. This error is increased in lower scattering regimes of reduced scattering coefficients of 0.5-1 (mm^{-1}). Simulations deviating anisotropy by 0.1 from true tissue value may incur error of up to 10% at reduced scattering coefficients of 0.5 (mm^{-1}).

Refractive index selection for Monte-Carlo simulation is typically centered around a value of 1.4. A range of values is often considered depending on tissue and wavelength selection where $1.35<n<1.5$. Within this range, simulation errors in absorption and scattering coefficients are almost linearly proportional to the difference in refractive index from true refractive index of sample. For example, simulating a value of 1.45 while the true tissue sample value is 1.4 will result in a 5% error in optical property extraction.

Absorption and scattering are a baseline axis where data simulation density is the primary consideration. For example, if a data value falls between two absorption simulation values interpolation is needed. Increasing computing speeds and optimizations within Monte Carlo simulations allow step sizes between absorption and scattering values to be small due to an increased number of simulations. Such step sizes for absorption coefficient simulations are often as small as 0.0005/cm and scattering coefficient step sizes of 0.01-0.02. Several methods for extracting absorption and scattering coefficients from diffuse reflectance have been theorized, each with benefits. Interpolation of two diffuse reflectance values into a 4D data cube is a common method relying on a series of moderate step size simulations of absorption and scattering coefficient combinations.[17] This technique of interpolating to adjacent known optical properties has the primary benefit of reducing simulation processing during creation of the LUT. Another technique is a hyper-dense linear LUT to rapidly estimate absorption and scattering without computationally taxing interpolation processes labeled “Linear Rd”. With this dense linear method absorption and reduced scattering coefficients values are found with rounding to adjacent data points.[17] Finally, a third method of fitting the simulated data sets to an analytical function is shown below labeled 2-D Fit. (Fig. 9) In this method diffuse reflectance values are evaluated with the analytical function modeling the optical property data.

Estimation of optical properties in this technique occurs rapidly much akin to the dense linearized LUT however, minor error up to 4% is associated with this analytical technique.[14]

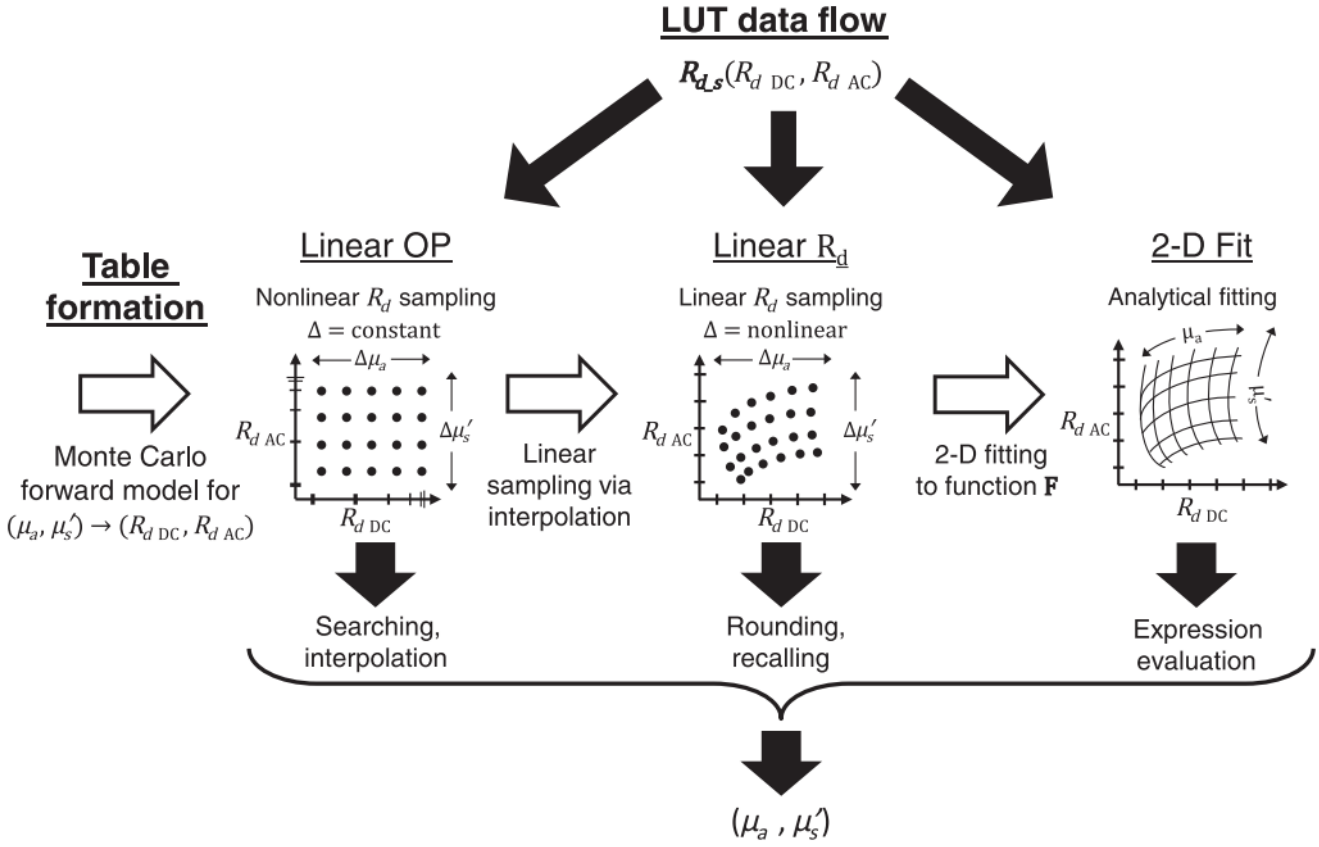

Figure 9: LUT protocols: black arrows indicate data flow for each technique and white arrows indicate additional steps in LUT creation processing. Adapted from Ref. 17

Experimental Error

Within a real data set there are numerous potential sources of error, in this section more consistent quantitative examples of error are presented. Quantified errors presented are projection boundary effects, binning of data, height calibration deviation, and spatial frequency projection error. Notable errors that will not be quantified are effects of movement, optical phantom inaccuracies, ambient noise variations, topography of sample, and relative camera angle to sample.

Projection boundary effects need to be considered when imaging with any finite projection area. A large projected area relative to sample region causes edge effects to be irrelevant, however when imaging an area of

interest close to the size of the projection, values near the border will inherently carry error. This error is described as a reduction in diffuse reflected light due to projected light scattering out from the projection region. Points central to the projection maintain diffuse reflected light values by both losing to and gaining from light in surrounding areas. Error from projection boundaries is heavily affected by absorption and scattering regime of sample. Values within 2cm from the projection edge may be subject to error in reflectance of >1% depending on optical properties of tissue.[14]

Binning is a common practice to reduce pixel noise by averaging adjacent pixel values into a single pixel. Careful use of binning in raw data is required for SFDI due to the necessity of several sampling points within a spatial frequency oscillation. An equation to calculate percentage error for AC reflectance values is presented in Eq. 4**.** Where x is number of pixels per bin, N is number of pixels in one-dimension, l is the corresponding projection length in millimeters, and f is the spatial frequency of the AC signal.[14]

$$\delta R_{Binning} = 209\left(\frac{flx}{N}\right)^{2.113} \quad (4)$$

Height adjustment is critical to maintaining calibrated intensity values and a focused camera image. When calibrating with a phantom data set, inconsistent distances from camera head to sample may alter pixel intensity values relative to the calibration measurement. This varied intensity would then propagate to error within the diffuse reflectance estimate during data analysis. An equation for relative percent error in optical properties is shown in Eq. 5, where r is the camera aperture radius in cm, is height of camera from sample, and x is deviation in height from focus. In low scattering and high absorption regimes the error due to height variation is reduced. However, even a small change of 1mm may result in 2-5% error for optical properties, therefore careful consideration and control should be done to ensure accurate height adjustment.[14]

$$\delta R_{Height} = -\frac{200r}{h^2}\frac{\cos\left(\frac{r}{h}\right)}{\sqrt{1-cos^2\left(\frac{r}{h}\right)}}x \quad (5)$$

Spatial frequency projection accuracy is vital to data collection especially when using a single spatial frequency. In the case of a single spatial frequency with a planar image error within the projection pattern is linearly proportional to relative error in absorption and scattering coefficients. For example, an error of 10% in the projected pattern would result in a proportional 10% error in estimated optical properties. Surface geometry may impact projection accuracy due to warping of pattern and therefore must be accounted for. Profilometry is often used to account for sample topography by using pre-defined modifiers based on height difference from focused height.

Many errors arise when working with real data collection. One benefit of SFDI in mitigating error is the use of calibration with a known optical phantom to remove hardware effects, ambient lighting, and height deviation from diffuse reflectance values. There are many potential effects on data acquisition and analysis both in the real and simulated domain. Even through these potential error sources, many uses of SFDI have been found and validated. These findings will be presented below.

SFDI Applications

SFDI techniques have been used widely since the early 2010's to quantify biologically relevant chromophores in a variety of potential applications. Quantifying burn healing response has been studied using SFDI multiple times in tissue models.[2,3] In both referenced articles they concluded a potential use for the quantified scattering coefficient values as an indication for tissue damage and structural change (Fig. 10). Another widely studied use for SFDI is the quantification of perfusion metrics for vascular assessment.[4,5] Those publications rely on estimated absorption coefficients to determine hemoglobin concentrations and from those concentrations, regional oxygen saturation. (Fig. 11) SFDI is recommended by the authors for extremity perfusion quantification in each case. Further development and improvement of the technique is also recommended to increase sensitivity and specificity in targeted tissues. An open source inexpensive platform (OpenSFDI) of this technique has been made available with complete instructions online to encourage further research in this field.[19] In the coming chapters we will analyze two additional applications of SFDI: microneedle tissue response and diabetic neuropathy perfusion testing.

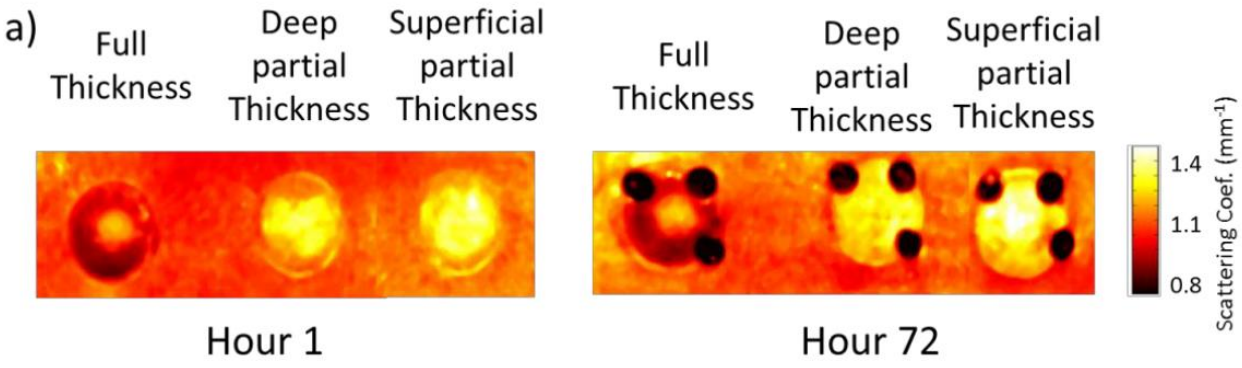

Figure 10: Representative images of the reduced scattering coefficient for the three burn categories at hour 1 and hour 72. Adapted from Ref. 2.

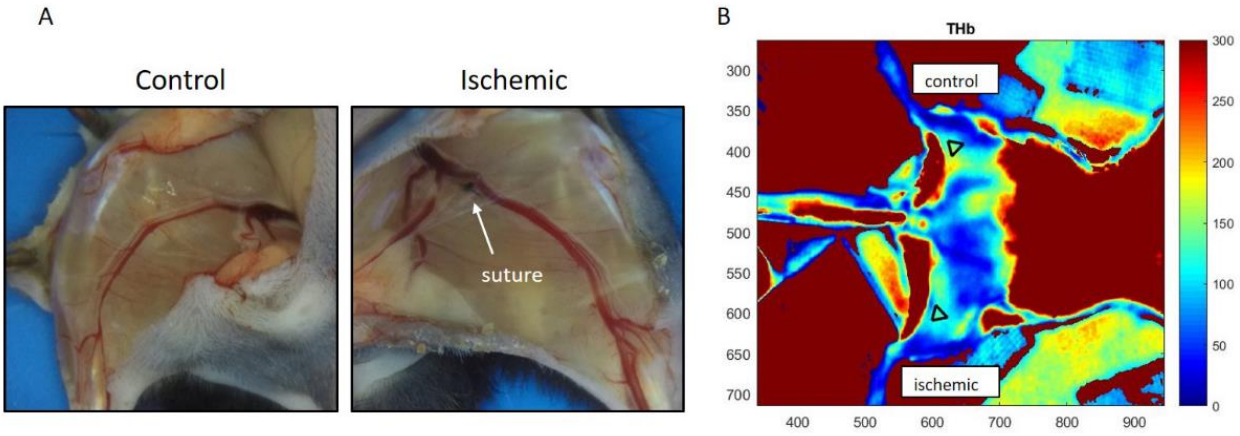

Figure 11: Example case of perfusion sensitivity: "A) Exposed vasculature of control and ischemic murine hindlimbs from one of n = 9 mice 28 days post-ligation. Suture (right) is placed right below the iliac arteries between the femoral nerve and vein. B) Example of ROI selection using custom MATLAB script on SFDI image." Adapted from Ref. 5

Chapter 1 References

1. Pogue, B. W. (2018, January 22). Optics of Medical Imaging. Retrieved May 14, 2022, from https://spie.org/news/spie-professional-magazine-archive/2018-january/optics-of-medical-imaging?SSO=1

2. Ponticorvo, A., Burmeister, D. M., Yang, B., Choi, B., Christy, R. J., & Durkin, A. J. (2014). Quantitative assessment of graded burn wounds in a porcine model using spatial frequency domain imaging (SFDI) and laser speckle imaging (LSI). *Biomedical Optics Express*, *5*(10), 3467. https://doi.org/10.1364/boe.5.003467

3. Mazhar, A., Saggese, S., Pollins, A. C., Cardwell, N. L., Nanney, L., & Cuccia, D. J. (2014). Noncontact imaging of burn depth and extent in a porcine model using spatial frequency domain imaging. *Journal of Biomedical Optics*, *19*(8), 086019. https://doi.org/10.1117/1.JBO.19.8.086019

4. Weinkauf, C., Mazhar, A., Vaishnav, K., Hamadani, A. A., Cuccia, D. J., & Armstrong, D. G. (2019). Near-instant noninvasive optical imaging of tissue perfusion for vascular assessment. *Journal of Vascular Surgery*, *69*(2), 555–562. https://doi.org/10.1016/j.jvs.2018.06.202

5. Leyba, K., Vasudevan, S., O'Sullivan, T., & Goergen, C. (2020). *Spatial frequency domain imaging of hemodynamic parameters in a murine model of hindlimb ischemia*. *February*, 11. https://doi.org/10.1117/12.2541944

6. Li, Y., Guo, M., Qian, X., Lin, W., Zheng, Y., Yu, K., Zeng, B., Xu, Z., Zheng, C., & Xu, M. (2020). Single snapshot spatial frequency domain imaging for risk stratification of diabetes and diabetic foot. *Biomedical Optics Express*, *11*(8), 4471. https://doi.org/10.1364/boe.394929

7. Rohrbach, D. J., Muffoletto, D., Huihui, J., Saager, R., Keymel, K., Paquette, A., Morgan, J., Zeitouni, N., & Sunar, U. (2014). Preoperative Mapping of Nonmelanoma Skin Cancer Using Spatial Frequency Domain and Ultrasound Imaging. *Academic Radiology*, *21*(2), 263–270. https://doi.org/10.1016/j.acra.2013.11.013

8. Laughney, A. M., Krishnaswamy, V., Rice, T. B., Cuccia, D. J., Barth, R. J., Tromberg, B. J., Paulsen, K. D., Pogue, B. W., & Wells, W. A. (2013). System analysis of spatial frequency domain imaging for quantitative mapping of surgically resected breast tissues. *Journal of Biomedical Optics*, *18*(3), 036012. https://doi.org/10.1117/1.jbo.18.3.036012

9. Hayakawa, C. K., Karrobi, K., Pera, V., Roblyer, D., & Venugopalan, V. (2018). Optical sampling depth in the spatial frequency domain. *Journal of Biomedical Optics*, *24*(07), 1. https://doi.org/10.1117/1.jbo.24.7.071603

10. Gioux, S., Mazhar, A., & Cuccia, D. J. (2019). Spatial frequency domain imaging in 2019: principles, applications, and perspectives. *Journal of Biomedical Optics*, *24*(07), 1. https://doi.org/10.1117/1.JBO.24.7.071613

11. Lepelaars, E. S. A. M. (1996). Electromagnetic pulse distortion in living tissue. *Medical and Biological Engineering and Computing*, *34*(3), 213–220. https://doi.org/10.1007/BF02520076

12. Mazhar, A., Dell, S., Cuccia, D. J., Gioux, S., Durkin, A. J., Frangioni, J. V., & Tromberg, B. J. (2010). Wavelength optimization for rapid chromophore mapping using spatial frequency domain imaging. *Journal of Biomedical Optics*, *15*(6), 061716. https://doi.org/10.1117/1.3523373

13. Erfanzadeh, M., Nandy, S., Kumavor, P. D., & Zhu, Q. (2018). Low-cost compact multispectral spatial frequency domain imaging prototype for tissue characterization. *Biomedical Optics Express*, *9*(11), 5503. https://doi.org/10.1364/boe.9.005503

14. Bodenschatz, N., Brandes, A., Liemert, A., & Kienle, A. (2014). Sources of errors in spatial frequency domain imaging of scattering media. *Journal of Biomedical Optics*, *19*(7), 071405. https://doi.org/10.1117/1.jbo.19.7.071405

15. Tabassum, S., Pera, V., Greening, G., Muldoon, T. J., & Roblyer, D. (2018). Two-layer inverse model for improved longitudinal preclinical tumor imaging in the spatial frequency domain. *Journal of Biomedical Optics*, *23*(07), 1. https://doi.org/10.1117/1.jbo.23.7.076011

16. Neel Joshi, Craig Donner, and Henrik Wann Jensen, "Noninvasive measurement of scattering anisotropy in turbid materials by nonnormal incident illumination," Opt. Lett. 31, 936-938 (2006)

17. Angelo, J., Vargas, C. R., Lee, B. T., Bigio, I. J., & Gioux, S. (2016). Ultrafast optical property map generation using lookup tables. *Journal of Biomedical Optics*, *21*(11), 110501. https://doi.org/10.1117/1.jbo.21.11.110501

18. Prahl, S. (n.d.). *Optical Absorption of Hemoglobin*. Optical absorption of hemoglobin. Retrieved May 30, 2022, from https://omlc.org/spectra/hemoglobin/

19. *SFDI 101*. Open SFDI. (n.d.). Retrieved June 11, 2022, from http://opensfdi.org/sfdi-101/

CHAPTER 2

Perfusion Reactivity Analysis of Microneedle Treatment

Introduction

Needles have been used for millennia as ancient rituals or for claimed medical benefits.[1] A modern interpretation of this practice originated as manufacturing accuracy and capabilities increased throughout the 20th century. The first commercially available microneedle, as we understand today, was created in Germany in the early 1900's with the claim to treat acne and skin scarring.[2] From this commercial inception another progression occurred, the inclusion of an electric motor to move the microneedle. This advancement was done by dermatologist Ernst Kromayer in 1905 with the claim of treating birthmarks, hyperpigmentation, and scarring. Jumping forward to 1990's a new focus for microneedles was found, inducing collagen production cosmetically to reduce wrinkling of age.[3]

Today microneedles are being used for many different applications depending on microneedle structure such as hollow needles, needle geometry, needle material (such as dissolvable, drug loaded, etc.) and needle length (Fig. 12).

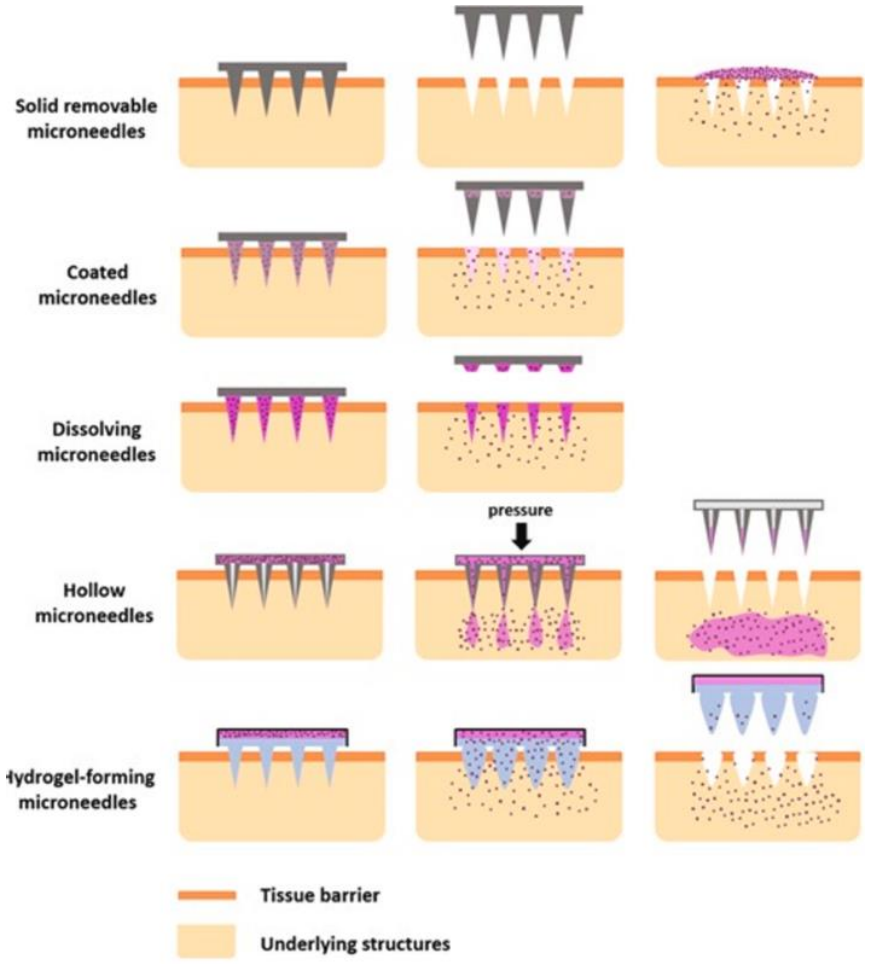

Figure 12: Microneedle application methods for drug delivery. Adapted from Ref. 5.

Many dermatological uses for microneedles rely on the simple mechanism of the microneedles piercing the skin causing reconstruction cycles within the tissue to repair the region or increasing medication penetration into skin.[3] Since 2000, many commercial and research microneedling instruments have been developed. Dermaroller, derma-stamp, dermapen, Radiofrequency microneedle devices, drug delivery, dissolvable, and light emitting microneedles are all examples of varied techniques on the same technological basis of microneedles.[4,5,6] The penetration of microneedles range between 0.2mm-3.5mm depending on their intended use. For example, Beauty Mouse® for home use has 400 needles each of approximately 0.2mm in length on a rolling surface.[7] Radiofrequency microneedle devices can be up to 3.5mm to allow for specific dermis layer targeting of treatment.[4]

When constructed with hollow needles, microneedles can extract interstitial fluid (ISF).[8,9] ISF can be a source of important biomarkers relevant to disease and health states. Currently one of the easiest methods of extracting ISF is creating a vacuum blister on the skin then extracting fluid from the created blister. Microneedles can also be used to extract this ISF over time, in some cases requiring overnight application into tissue to collect ISF. Inversely microneedle patches for medication delivery are being tested for a minimally invasive method of introducing drugs or vaccines through diffusion inside of dermal tissue as opposed to an injection into muscle tissue.

With all these valuable medical and cosmetic uses of microneedle arrays, methods of action have yet to be fully elucidated. The widely accepted mechanism of microneedle treatment is the creation of microinjuries in superficial capillaries which trigger cells to release signaling molecules (ex. Bradykinins and histamine). These signaling molecules affect DNA expression in neighboring cell's DNA to increase expression of growth factors thereby healing and restructuring the region.[3] This bleeding causes a tissue healing cascade activating proteins and growth factors. Often scar tissue, when treated with microneedles, revascularizes and begins creation of a new intercellular matrix. [4] We believe the use of SFDI to quantify hemoglobin changes in a region of microneedle treatment can be a valuable tool to better understand the physiological response from microneedle treatment and pressure application. Pressure application has been well documented to activate physiologic response to repair tissue.[3] Two such responses are post occlusive reactive hyperemia (PORH) and pressure induced vasodilation (PIV) which may play a large role in observed physiologic mechanisms. PORH describes the initial peak and period of sustained hemoglobin concentration following occlusion release. (Fig 13) PIV is a protective cutaneous response that aids in vascular homeostasis during low pressure application (Fig 14**).**

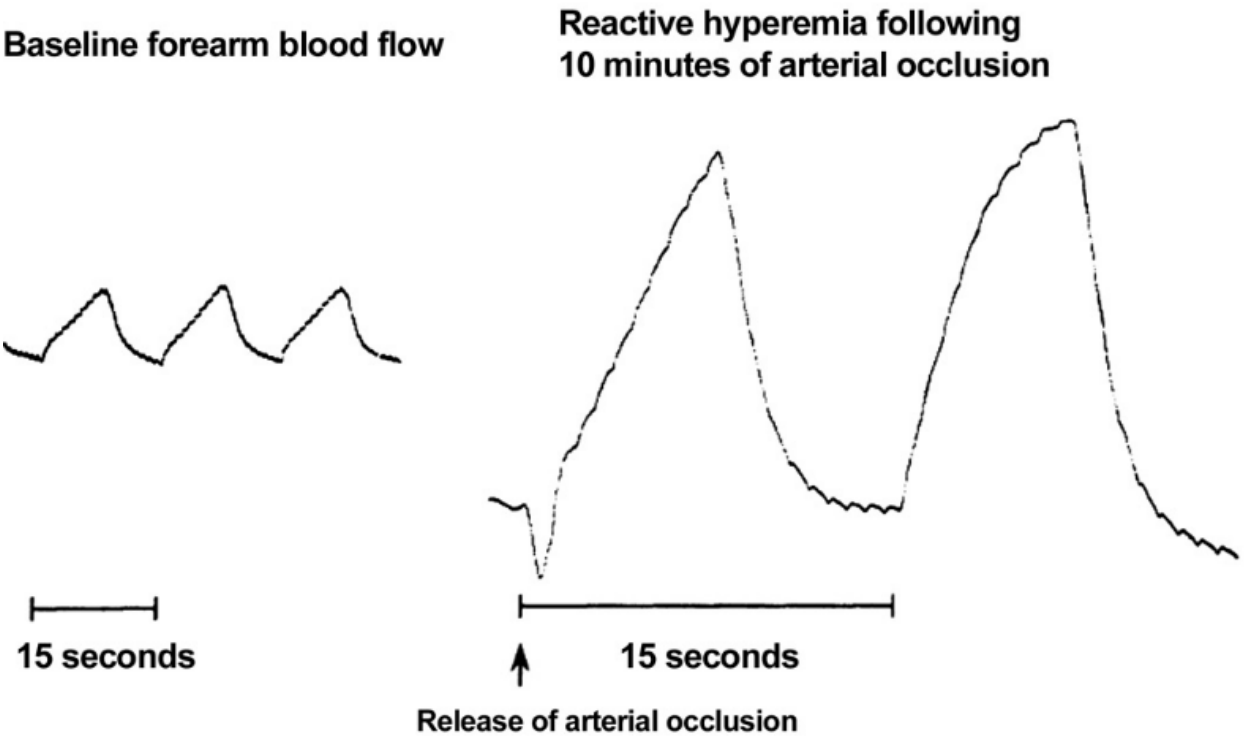

Figure 13: Example of reactive hyperemia, (Left) baseline blood flow, (Right) blood flow action following arterial occlusion release. Adapted from Ref. 10

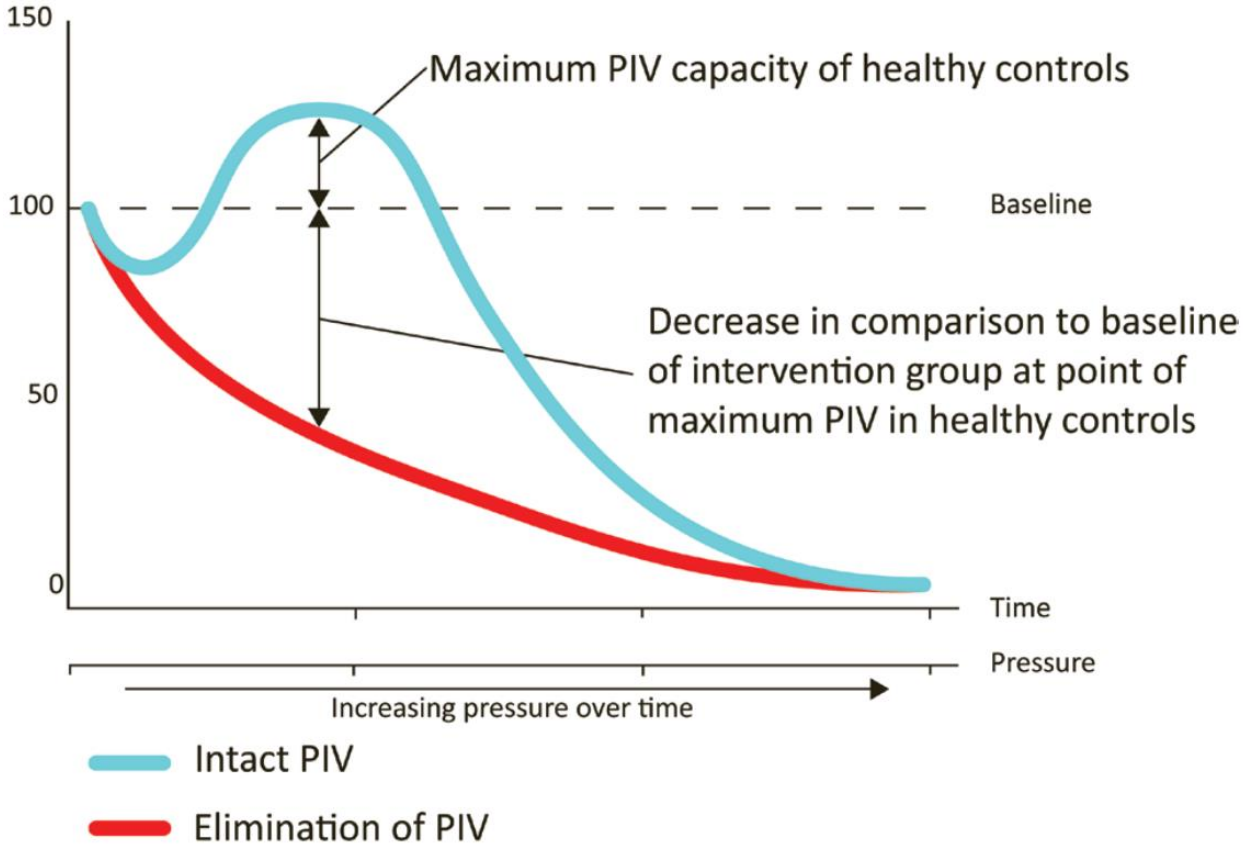

Figure 14: Perfusion curves during loading with increasing pressure in subjects with and without pressure-induced vasodilation. Adapted from Ref. 10

We sought to better understand the short-term physiologic response to microneedle application and quantify the response using Spatial Frequency Domain Imaging (SFDI). In the coming pages we will discuss relevant anatomy, experimental methodology, physiologic response to pressure, and SFDI quantified results from microneedle testing response.

Microneedle Relevant Anatomy & Physiology

To better understand the anatomical system and results, it is key to put known variables into context. As previously stated, microneedles can range in length from 0.2-3.5mm which drastically changes the targeted region of treatment. Dermis penetration has been identified as a depth to begin the repair of scar tissue. Even micro-needling of superficial wounds activates inflammatory mechanisms to aid in epithelial migration.[3] In this section we will

describe with available quantitative detail layers of the skin and physiological response to perturbation such as microneedle wounds. All following anatomical statements are generalities which may vary dependent on the person, medical conditions, region of the body, and more.

Epidermis

The epidermis is often subdivided into 4 primary regions from superficial to proximal: Stratum Corneum, Stratum Granulosum, Stratum Spinosum, and Stratum Germinativum. Each layer is differentiated by varied cell types attributing to each layer's function. Epidermal tissue can range from 0.05-0.6mm thick depending on the region of the body and other factors such as disease state. For example, the thickness of the epidermis in the eyelid being roughly 0.1mm thick in comparison to the heel of the foot up to 0.6mm[11].

Cornified Layer (Stratum Corneum) is composed of corneocytes known as horny cells used as mechanical protection for the deeper layers of the epidermis. The horny cells are rich in protein, low in lipid content, and are considered dead due to loss of nuclei. These dead cells stack give a barrier for water penetration and are fully shed and replaced approximately every 30 days. This layer as seen in figure 15 is the smooth in appearance top layer of the epidermis.

Granular Layer (Stratum Granulosum) contains living cells containing keratohyalin granules and are responsible for protein synthesis for keratinization. The thickness of this layer ranges from 1-3 cells thick up to 10 times as thick depending on the region of the body the skin is found. Horny cells are created in this region as cells from the granular layer proliferate, they undergo dissolution of cellular organelles to create the dead horny cells of the stratum corneum. This layer can be seen in figure 15 as what appears to be the interface between the stratum corneum and the below cellular region.

Squamous Cell Layer (Stratum Spinosum) has a variety of cell types with different properties and cellular structure depending on location. This layer often is between 5-10 cells thick and is an active region for chemical signaling and enzymatic action. The method of enzymatic action is lamellar granules found within the spinous cells that make up this layer. These lamellar granules serve additionally, to deliver precursors for stratum corneum lipids to the intercellular space. This layer in figure 15 is identified as the largest section of the epidermis as shown.

Basal Layer (Stratum Basale) consists of a single layer of columnar keratinocytes perpendicular to the dermis. These cells often have elongated nuclei and contain melanin pigment from adjacent melanocytes. Cell proliferation occurs in this layer within clonogenic stem cells to repair and maintain the more superficial layers of the epidermis. Upper blood net capillaries supply blood to this base layer of the epidermis. Finally, the basal layer bonds with the dermis due to intertwining collagen fibers making up the basement membrane. The basement membrane interfaces between the epidermis and dermis allowing fluid and cells through its porous surface.

Dermis

The dermis tissue is composed largely of several biological elements of vasculature, nerves, musculature, secretory cells, and connective tissues. Approximately 70% of skin's dry weight is due to collagen specifically type 1 collagen. Macrophages, mast cells, and other blood born cells enter dermal tissue in response to stimuli. Depending on external stimuli; flow regulation, secretions, and cell replication are all properties maintained in homeostasis by interaction with the epidermis. This region of the skin ranges from 1-4 millimeters.

Vasculature (subpapillary & superficial plexus) can be found in 2 regions; the superficial plexus is superficial within the dermis close to the basement membrane-dermis junction. In comparison, the subpapillary vasculature can be found intertwined with the subcutaneous fat layer at the proximal edge of the dermal tissue. These 2 regions create the "upper/lower blood net" supply for the dermis tissue differentiating these regions often is of interest for quantifying tissue hemoglobin concentrations. Of note, the subpapillary plexus has notably larger vasculature in comparison to the superficial plexus. These vascular regions can be seen in figure 15 in the bottom right corner labeled "Dermal vasculature" where Deep plexus is equivalent to subpapillary.

Muscle Tissue is found as a component in the vasculature within the dermis across all areas of the body but also acts to control hair follicle movement. Skin specialized smooth muscle called glomus bodies can be found regulating body temperature and blood flow within the peripheral appendages, such as fingers or soles of feet. Skin on the face however has voluntary muscle allowing for facial expressions. An example of this tissue can be seen in figure 1 labeled "Arrector pili muscle".

Nervous Tissue is found primarily in neurovascular bundles within the dermis. This allows direct supply for the nerves within the subpapillary and superficial plexus. Meissner corpuscles within the dermis help mediate

touch sensation within the palm and fingers of the hand and base of the foot. Otherwise, other sensation such as pain, temperature, and itch, are transferred from the periphery to the central nervous system by unmyelinated nerve fibers around hair follicles, and the papillary dermis.

Mast Cells are secretory cells distributed in connective tissues such as the abundant collagen. They are present largely in the papillary dermis and subcutaneous fat below the dermal tissue. Mast cells express histamine, leukotrienes, prostanoids, proteases, cytokines, and chemokines to surrounding tissue and vasculature. These molecules have a key role in the inflammatory response and are directly tied to allergies, arthritis, and many other diseases.

Subcutaneous Fat

Being the deepest layer of the skin, the fat provides structure for underlying tissues while storing energy as fat cells. Much like the previous layers, function relies on location for subcutaneous fat such as acting as thermal and trauma insulation for vasculature and bone tissues. Subcutaneous fat is widely considered the thickest layer of skin while having the lowest absorption and scattering coefficient. The yellow proximal region of figure 1 is the subcutaneous fat region.

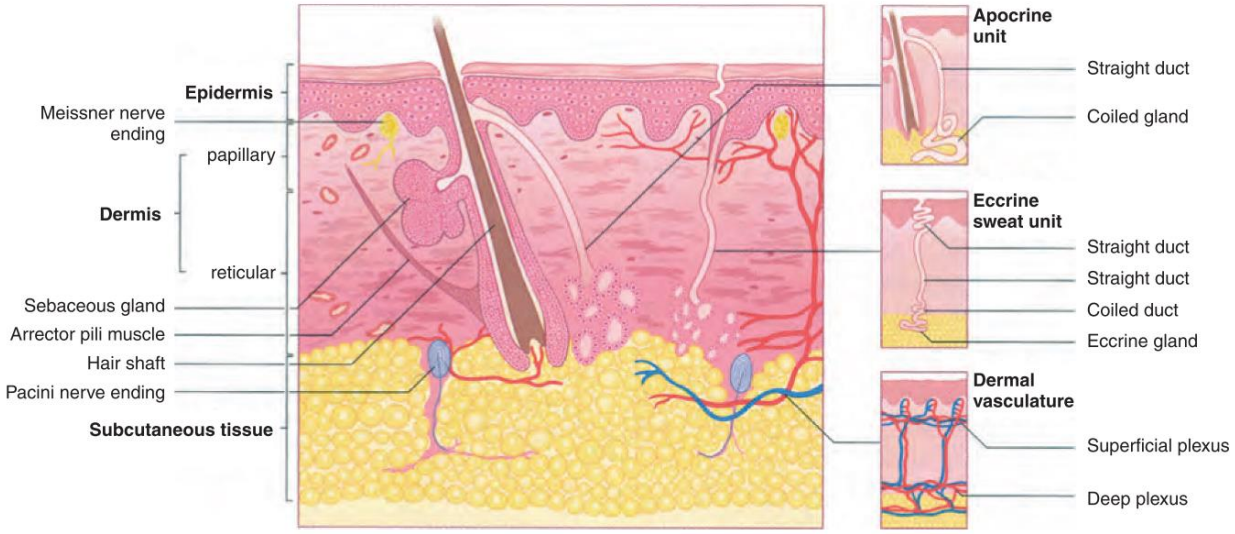

Figure 15: Skin anatomy cross-section: Adapted from Ref. 13 “Cross-Section of Skin and Panniculus”

Methods

Procedure

To prepare for data collection the Reflect RS system is calibrated using a phantom with known optical properties. During calibration and data collection all lights in the room were turned off to reduce ambient light noise. Height correction error was mitigated by focusing the SFDI system where the blank plate and microneedle would be placed on the skin. The testing region was indicated by using a permanent marker to create a square outline on the skin. (Fig. 16) These pre-acquisition steps aided in mitigating potential error in final chromophore values.

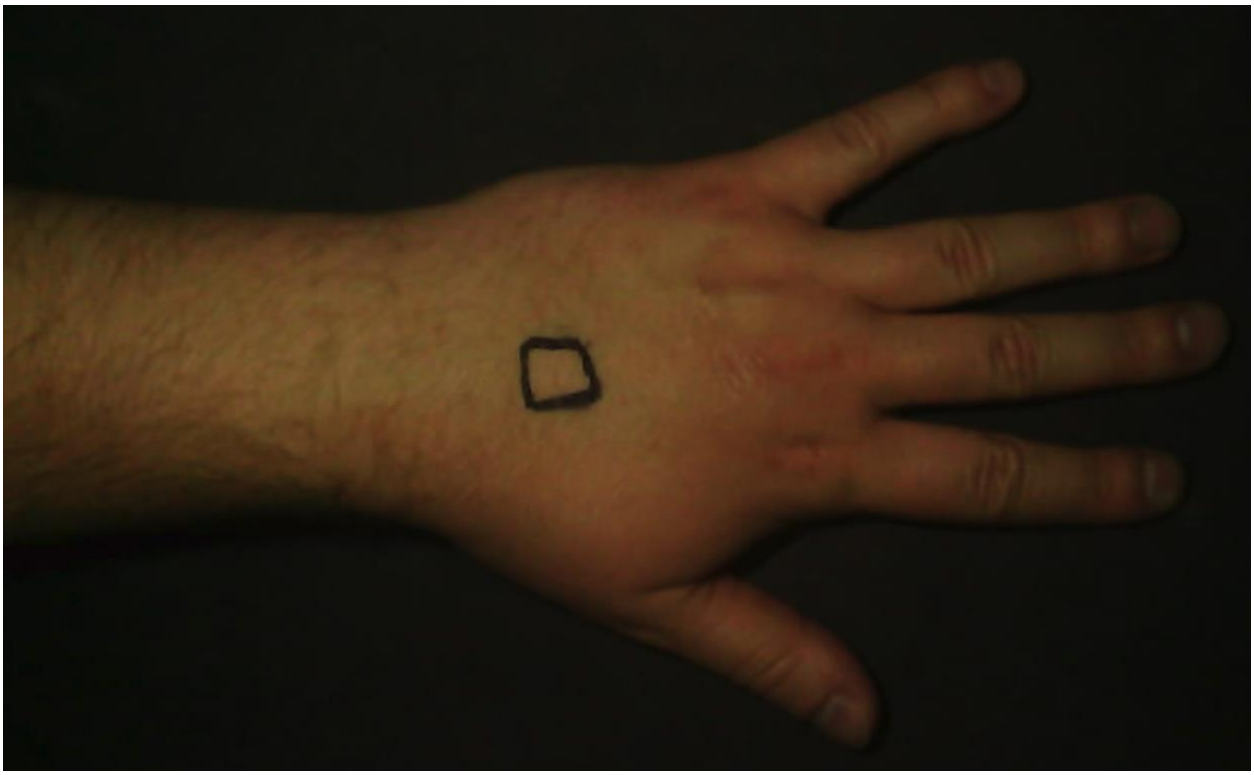

Figure 16: Example SFDI camera view of data collection for microneedle testing. The black square indicating the border of the metal plate where pressure is applied.

Each data collection ran for 10 minutes with an initial pre-treatment data collection to acquire a baseline value of the selected region. Upon completion of pre-treatment data, the blank plate is pressed into the back of the hand for 1 minute at a constant pressure of 0.5kg/cm^2 measured by a calibrated pressure Arduino placed onto the plate. Following this minute of pressure, the blank plate is removed, and a dataset is immediately collected. Then

each minute following additional datasets were collected up to ten minutes. (Fig 17) This time set gives changes over time to quantify pressure effects on the skin.

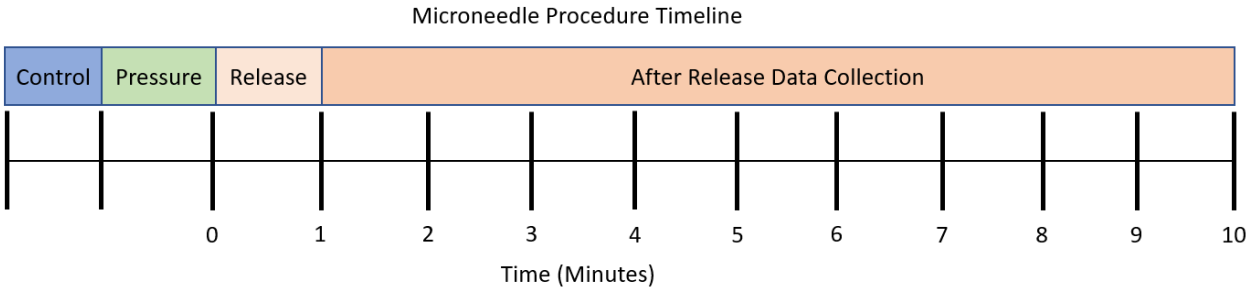

Figure 17: Microneedle procedure steps; Control value data collection followed by application and release of pressure. After release of pressure data is collected every minute for 10 minutes.

With the blank plate pressure series completed we investigated the effect of microneedle application alongside pressure under the same conditions at the same location. To ensure homeostasis in the testing region, a period of 30 minutes was given between blank plate testing and microneedle array application. A control value was collected followed by constant pressure of 0.5kg/cm^2 applied to the microneedle array on the back of the hand. Time series data was taken from the dorsum of the hand immediately upon pressure release and every minute thereafter. For volunteer safety microneedles were cleaned with heated acetic acid (normality of 17.4) between volunteer usage to remove biological tissues.

Materials

Microneedle Arrays used during testing were 1 cm^2 metal base plates with 400 μm tall microneedles pyramidal in shape with a square base 120 μm in width. This array was manufactured by the MicroInstruments & Systems Laboratory at the University of Maine. Additionally, blank metal plates of the same size were supplied for comparison with microneedle plates effect in the skin. Example blank plate and microneedle arrays are shown below. (Fig 18)

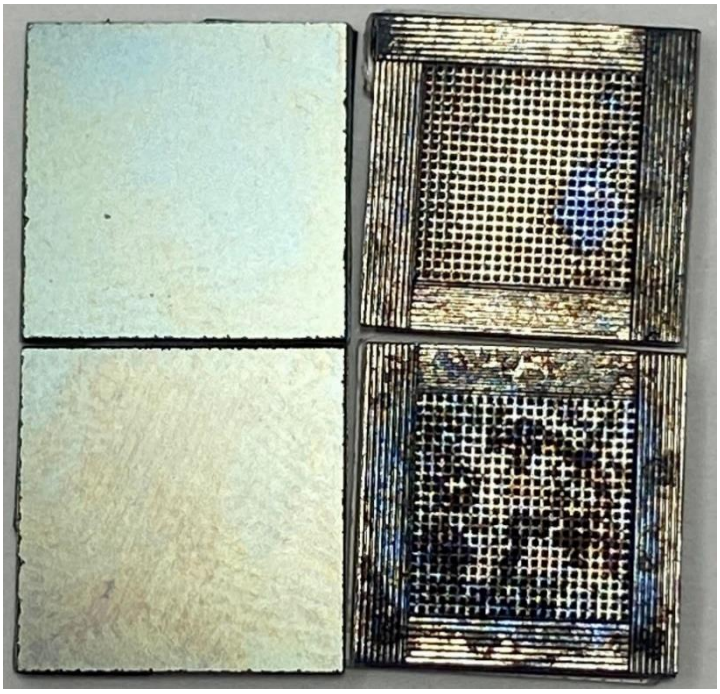

Figure 18: 1cm^2 blank and microneedle plates used in testing. Top plates are less used, bottom plate examples after many uses.

Pressure Arduino was used during testing to maintain constant pressure on the skin. External force applied to the sensor varies internal resistance allowing for calibration based on resistance readout to Arduino software. (**Fig 19)** The accepted range of pressure from manufacturer specifications was 0.1-10kg. The calibration range for this Arduino with a 0.99 r^2 fit value was 0.25-1.25kg/cm^2. The pressure Arduino configuration used is shown below. **(Fig 20)_**

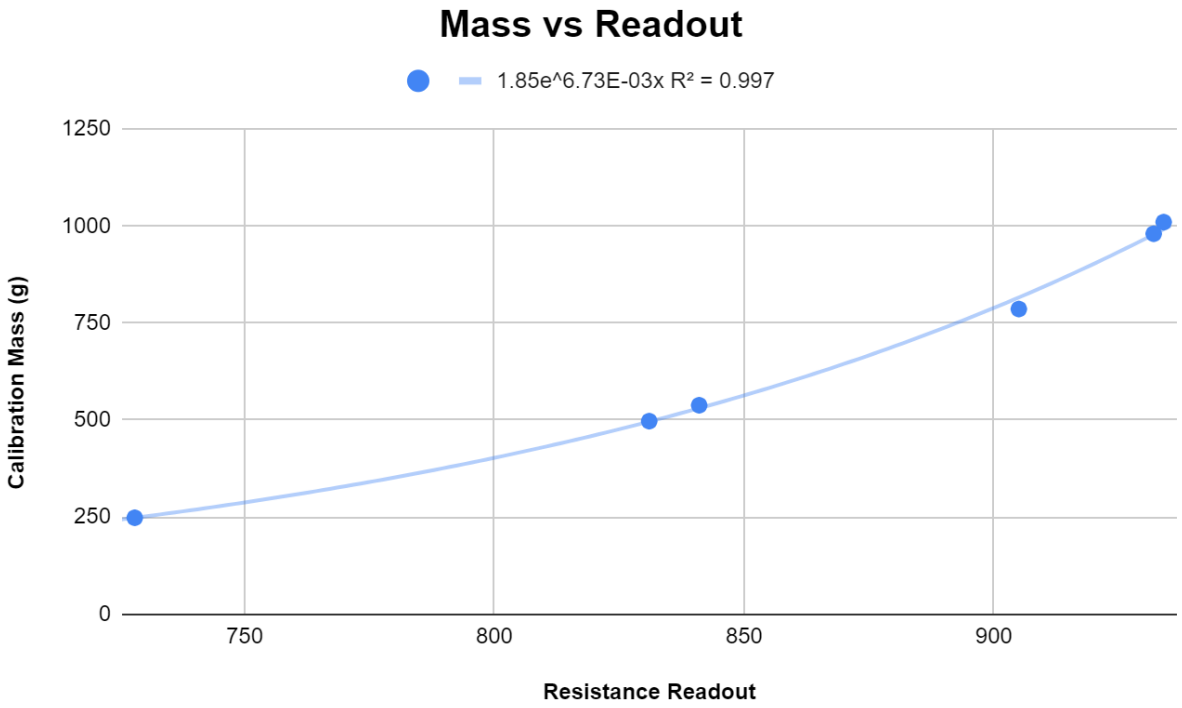

Figure 19: Calibration curve for pressure Arduino using multiple tested masses

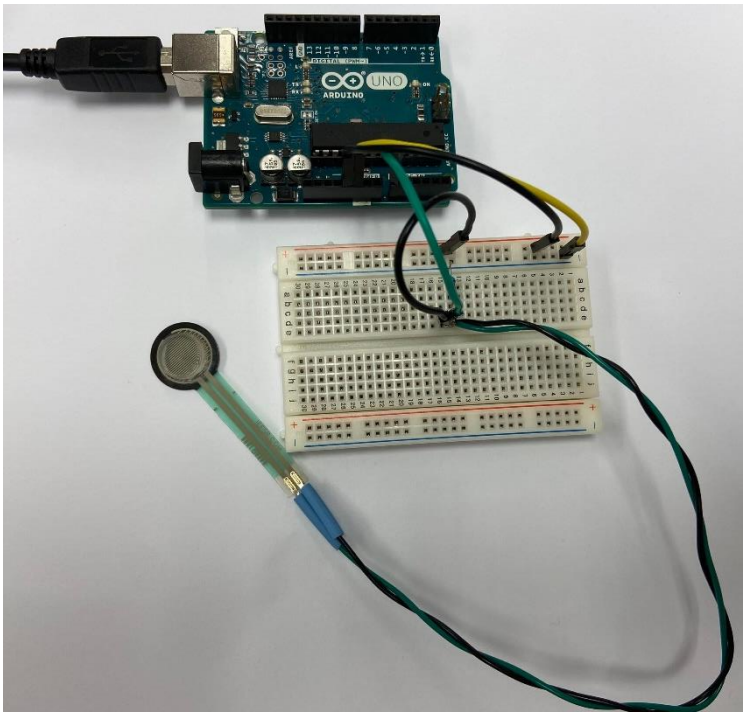

Figure 20: Pressure sensitive Arduino configuration with breadboard

Reflect RS is a commercial spatial frequency domain imaging technology, manufactured by Modulim, that uses visible and near infrared light to estimate pixel absorption and scattering coefficients and further extract regional chromophore concentrations. In this study we collected data using 2 spatial frequencies (0 and 0.1/mm) at the following wavelengths 659, 691, 731, 851nm. Each data collection time point took approximately 40 seconds to complete.

Results

The SFDI Reflect RS system was used for imaging the back of the hand in 2 volunteers, at 4 locations. For each participant 8 total time trial data sets were collected, 4 blank plate and 4 microneedle sets. Regional hemoglobin oxygen saturation and total hemoglobin values were found by custom MATLAB analysis code of the SFDI data. Both values are calculated using the equations shown below (Eq 6,7) where HbO2 is oxy-hemoglobin and HHb is deoxy-hemoglobin concentration output from MATLAB analysis. These values are used as physiological markers to characterize perfusion changes due to microneedle application. Time plots are presented (Fig 21-23) showing both total hemoglobin and regional oxygen saturation change over time for both volunteers.

Comparing initial release for participant 1 both blank plate and microneedle array using a Z-Score test yields a Z score of -1.06 and a p value of 0.14. However, participant 2 release value comparison of blank plate to microneedle array gave a Z score of -2.45 resulting in a p value of 0.007. With mixed statistical relevancy further data collection is required. All error bars presented are a standard deviation within the data set. No other time points from the presented data had a statistically significant p value.

Finally, total hemoglobin values are similar for both blank plate and microneedle testing. However, both sets of data to indicate an elevated total hemoglobin response relative to control values. The values presented below for total hemoglobin change are averaged values for both participants across all similar data sets. Similarly with regional oxygenation an initial peak can be observed post release increasing total hemoglobin by up to 10%.

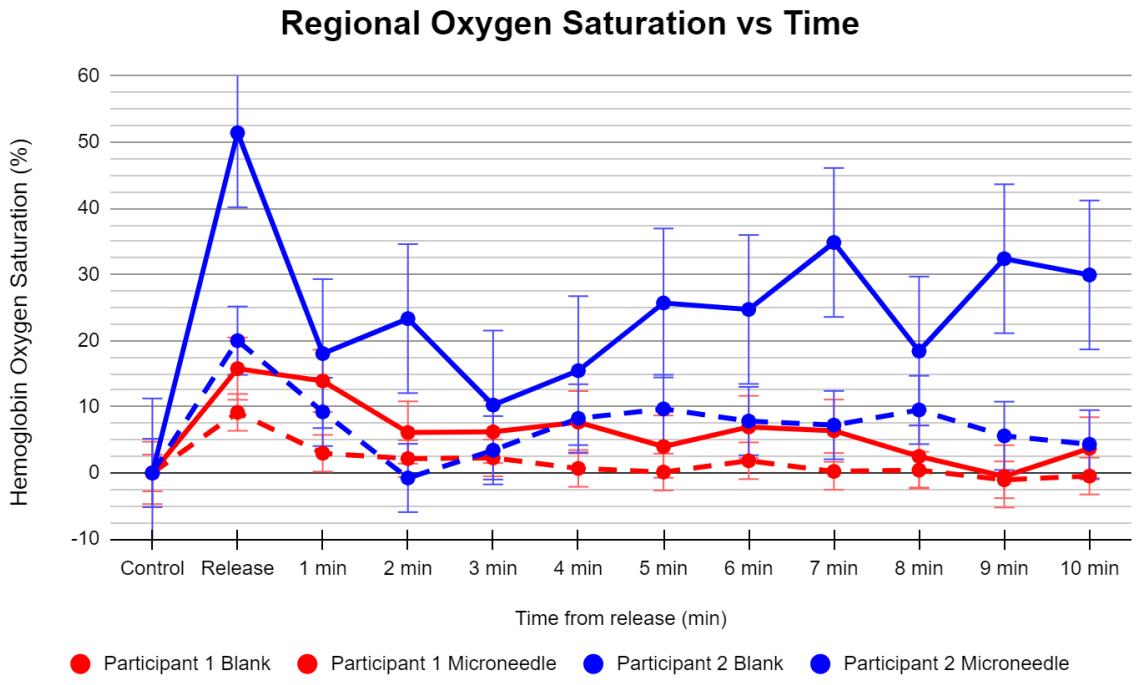

Figure 21: Averaged relative to control oxygen saturation in tested region of interest (15x15 pixels)

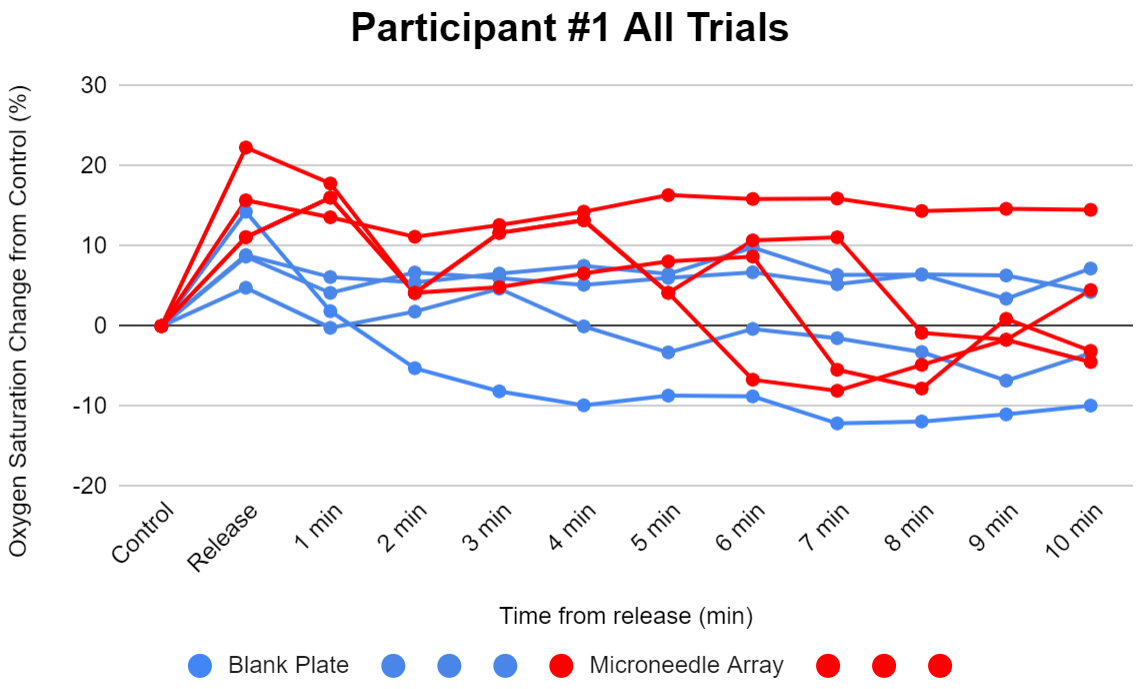

Figure 22: All averaged trial data for participant 1

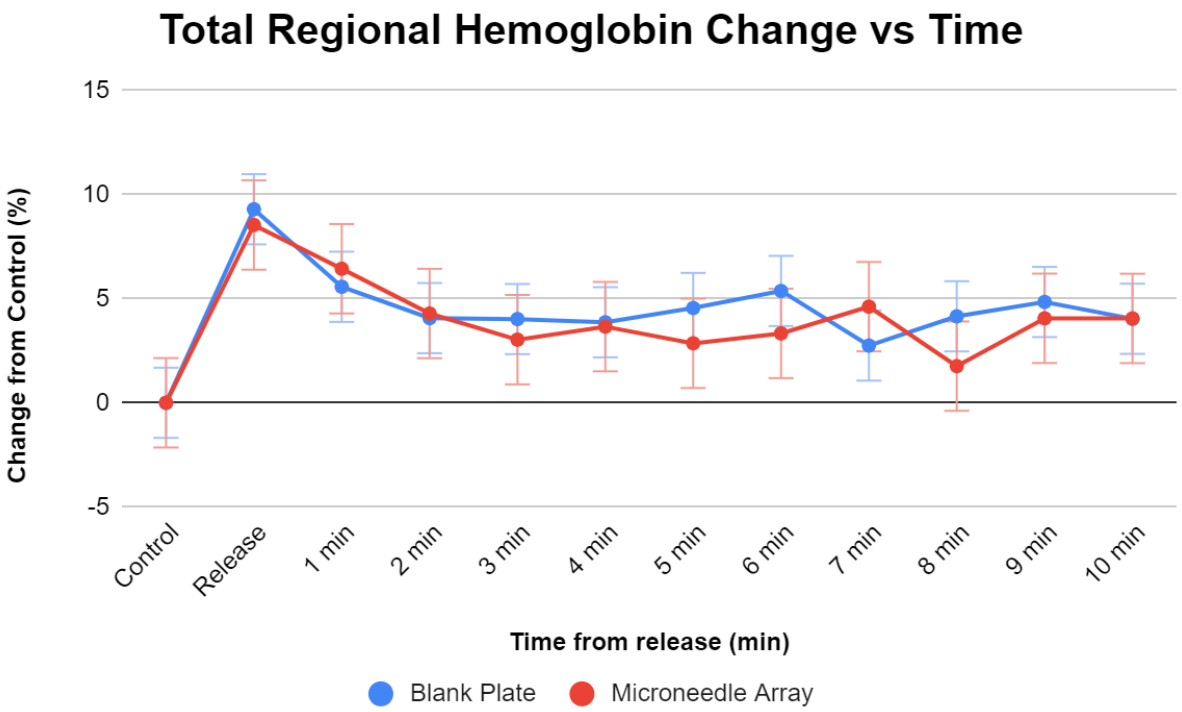

Figure 23: Total percent hemoglobin concentration (HbO2+HHb) change averaged for all participants relative to control

Discussion

From the presented results two key points may be observed; regional perfusion increases following pressure application and microneedle application increase of regional oxygenation. Regional oxygenation increases due to microneedle in comparison to blank plate can be observed in **figure 21.** Both participant 1 and participant 2 see a raised initial peak and a higher sustained average oxygenation in the test region when microneedles are applied. Total hemoglobin change due to pressure effects can be discerned from figure 23 where both microneedle and blank plate trials result in roughly the same elevation of perfusion. Total hemoglobin is calculated for the above graph by summing estimated oxy/de-oxyhemoglobin values for each time point relative to control values. (Eq. 6)

$$Hb_{total} = HbO2 + HHb \quad (6)$$

$$StO2 = \frac{HbO2}{Hb_{total}}$$

(7)

In this research we better understand the physiologic impact of pressure and microneedle penetration of the skin. These results are small scale and further testing is needed with larger sample populations and different regions of skin. There are several mechanisms that may describe the presented results: Post-Occlusive Reactive Hyperemia (PORH), Pressure-Induced Vasodilation (PIV), and oxygen diffusion through the microneedle site.[12] Time points within the data after pressure application may be positively affected by PIV. Directed pressure on the experimental region may elicit PORH due to occlusion of vasculature and consequent blanching.

Microneedling is a growing industry but in many ways lacks quantitative studies of physiologic changes. Further research is recommended to study varied pressure application, spatial frequency variation for depth sensitivity, sequential microneedle treatments, disease states, and different regions of tissue. These tests would elucidate the effects of pressure induced vasodilation, perfusion changes in the upper and lower blood net, and extended microneedle changes.

Blank Plate StO2 Averages (Participant #1)	Microneedle StO2 Averages (Participant #1)	Blank Plate StO2 Averages (Participant #2)	Microneedle StO2 Averages (Participant #2)
0	0	0	0
9.15%	15.77%	20.00%	51.43%
2.98%	13.92%	9.23%	18.05%
2.17%	6.11%	-0.76%	23.33%
2.26%	6.21%	3.43%	10.26%
0.68%	7.67%	8.25%	15.47%
0.14%	3.98%	9.68%	25.70%
1.85%	6.95%	7.84%	24.72%
0.23%	6.39%	7.23%	34.85%
0.43%	2.50%	9.52%	18.43%
-1.03%	-0.52%	5.61%	32.39%
-0.47%	3.72%	4.33%	29.93%

Table 1: Average StO2 changes by participant

Total Hb Changes from Control Blank Plate	Total Hb Change from Control Microneedle
0%	0%
9.30%	8.54%
5.57%	6.44%
4.07%	4.29%
4.02%	3.03%
3.87%	3.66%
4.55%	2.86%
5.37%	3.33%
2.75%	4.62%
4.15%	1.76%
4.85%	4.06%
4.04%	4.05%

Table 2: Total hemoglobin concentration change

Chapter 2 References

1) Lehmann H. Acupuncture in ancient China: how important was it really? J Integr Med. 2013 Jan;11(1):45-53. doi: 10.3736/jintegrmed2013008. PMID: 23464646.

2) *The history of microneedling and Facelifts*. MDPen. (2020, June 15). Retrieved April 29, 2022, from https://mdpen.co/the-history-of-microneedling-and-facelifts/

3) Liebl, H., & Kloth, L. C. (2012). Skin cell proliferation stimulated by microneedles. Journal of the American College of Clinical Wound Specialists, 4(1), 2–6. https://doi.org/10.1016/j.jccw.2012.11.001

4) Singh, A., & Yadav, S. (2016). Microneedling: Advances and widening horizons. Indian Dermatology Online Journal, 7(4), 244. https://doi.org/10.4103/2229-5178.185468

5) Cárcamo-Martínez, Á., Mallon, B., Domínguez-Robles, J., Vora, L. K., Anjani, Q. K., & Donnelly, R. F. (2021). Hollow microneedles: A perspective in biomedical applications. International Journal of Pharmaceutics, 599(March). https://doi.org/10.1016/j.ijpharm.2021.120455

6) Coppola, S., Vespini, V., Nasti, G., & Ferraro, P. (2021). Transmitting Light through Biocompatible and Biodegradable Drug Delivery Micro Needles. *IEEE Journal of Selected Topics in Quantum Electronics*, *27*(5). https://doi.org/10.1109/JSTQE.2021.3057834

7) Mccrudden, M. T. C., Mcalister, E., Courtenay, A. J., González-Vázquez, P., Raj Singh, T. R., & Donnelly, R. F. (2015). Microneedle applications in improving skin appearance. Experimental Dermatology, 24(8), 561–566. https://doi.org/10.1111/exd.12723

8) Rosenberry, R., & Nelson, M. D. (2020). Reactive hyperemia: A review of methods, mechanisms, and considerations. *American Journal of Physiology - Regulatory Integrative and Comparative Physiology*, *318*(3), R605–R618. https://doi.org/10.1152/AJPREGU.00339.2019

9) Samant, P. P., & Prausnitz, M. R. (2018). Mechanisms of sampling interstitial fluid from skin using a microneedle patch. *Proceedings of the National Academy of Sciences of the United States of America*, *115*(18), 4583–4588. https://doi.org/10.1073/pnas.1716772115

10) Zwanenburg, P. R., Backer, S. F. M., Obdeijn, M. C., Lapid, O., Gans, S. L., & Boermeester, M. A. (2019). A Systematic Review and Meta-Analysis of the Pressure-Induced Vasodilation Phenomenon and Its Role in the Pathophysiology of Ulcers. *Plastic and Reconstructive Surgery*, *144*(4), 669e-681e. https://doi.org/10.1097/PRS.0000000000006090

11) Maiti, R., Duan, M., Danby, S. G., Lewis, R., Matcher, S. J., & Carré, M. J. (2020). Morphological parametric mapping of 21 skin sites throughout the body using optical coherence tomography. *Journal of the Mechanical Behavior of Biomedical Materials*, *102*(April 2019). https://doi.org/10.1016/j.jmbbm.2019.103501

12) Balasubramanian, G. V., Chockalingam, N., & Naemi, R. (2021). The Role of Cutaneous Microcirculatory Responses in Tissue Injury, Inflammation and Repair at the Foot in Diabetes. *Frontiers in Bioengineering and Biotechnology*, *9*(September), 1–11. https://doi.org/10.3389/fbioe.2021.732753

13) Kolarsick, P., Kolarsick, M.A., & Goodwin, C. (2011). Anatomy and Physiology of the Skin. *Journal of the Dermatology Nurses' Association*, *3*, 203-213.

CHAPTER 3

Pilot Study Utilizing Spatial Frequency Domain Imaging to Analyze Diabetic and Neuropathic Feet

Christian Crane, MS Biomedical Engineering, University of Maine

Karissa Tilbury, PhD Biomedical Engineering, University of Maine

Todd O'Brien, DPM, Penobscot Community Health

No authors or participants have any business interest or potential for personal gain from any organization or group associated with the following study. The authors believe that no real, potential, or apparent conflict of interest is known.

Abstract

Objective:

Prevention and treatment of neuropathy requires early, safe, and quantifiable techniques for medical intervention. In this pilot study, we examine the feasibility of spatial frequency domain imaging (SFDI) as a quantitative tool for plantar neuropathy risk stratification.

Method:

A small-scale pilot study was conducted with participants from four categorized demographics: healthy-young (20-48 yrs), healthy-old (50-65+ yrs), diabetic (59-67 yrs), and neuropathy (56-71 yrs). Each participant went through the same postural series (prone, elevated, reclined) while spatial frequency domain images (SFDI) of the plantar region of the foot were acquired. The images were then analyzed to estimate regional perfusion metrics including StO2 and papillary/reticular hemoglobin concentration of the 3rd metatarsal head and median values of the foot including heel.

Results:

In all participants, elevation of the foot resulted in decreased hemoglobin perfusion in both the papillary and reticular dermis layers. Neuropathy participants were found to have higher total plantar hemoglobin in all positions relative to other participant classes. These participants also had higher variance in their hemoglobin concentrations relative to healthy subjects.

Conclusion:

The postural regulation of perfusion appears correlated with disease progression and showed a potential application of SFDI as a noninvasive, rapid, and quantitative test. Participant group data indicates further investigation into postural perfusion is recommended for earlier detection of disease and as a qualitative healing metric.

Introduction

In 2019, the global prevalence of diabetes was 9.3% and current predictions estimate that by 2030 diabetes will impact 10.2% of the population with an alarming increase in prevalence in children, teens, and young adults.[1,2] Nearly 50% of all diabetic patients experience neuropathy with associated complications including: 1) abnormal sensations (paresthesia, allodynia, hyperalgesia, and spontaneous pains), 2) amputations, 3) bone damage and 4) microvascular dysfunction.[3,4,5] Peripheral arterial disease (PAD), is common in diabetic disease progression leading to decreased vascular function.[6] Chronic vascular damage often leads to ulcer formation and further necrosis on the plantar surface of the foot in high pressure regions such as the 1st, 3rd, 5th metatarsal heads and the heel.[7] Degradation of plantar tissue causes up to 25% of diabetic ulcer patients requiring some form of amputation.[8,9,10]

Diabetic neuropathy and ulcer formation are complex with many physiologic mechanisms under investigation.[11] Chronic hyperglycemia induces tissue damage through metabolic and oxidative stress such as polyol pathway, advanced glycation end products and protein kinase C activation.[12] Common vascular complications of diabetes progression include capillary steal syndrome, atherosclerosis, blood pooling and related ulcer formation.[13,14] Impaired metabolic and vascular function increases the propensity of ulcer formation via damage to peripheral C-fibre nerves due to inflammatory stress, ischemia, vascular insufficiency, and other factors.[5,15,16,17] Tissue damage as outlined above perpetuates risk for infection following ulcer formation leading to negative outcomes.

Early detection of ulcer formation and noninvasive quantification of disease progression is key to successful clinical intervention.[4,17,18] The gold standards of neuropathy risk stratification are nerve conduction velocity tests and tissue biopsy for epidermal nerve fiber density. Other widely used diagnostic techniques are monofilament testing, tuning fork, temperature perception, reflex testing, and ocular nerve counting.[9,19,20] Microcirculatory response to external stimuli such as pressure, occlusion, and temperature, is often muted in diabetic neuropathy patients resulting in reduced healing.[4] Nervous tissue degradation is irreversible necessitating a call for earlier detection to improve opportunities to employ preventative strategies. [16,21,22] Recently, diffuse optical imaging has been used for low cost, non-invasive quantitative investigation of perfusion metrics associated with diabetes and diabetic neuropathy.[23,24]

Existing optical techniques include laser Doppler flowmetry (LDF), laser speckle contrast imaging (LSCI), hyperspectral imaging, diffuse optical spectroscopy imaging (DOSI) and spatial frequency domain imaging (SFDI).[25,26,27,28,29,30] Both LDF and LSCI provide regional blood flow measurements to correlate with tissue perfusion. Hyperspectral imaging utilizes a continuous band of wavelengths for spectral analysis, comparatively SFDI is a wide-field, non-contact technique projecting discrete wavelengths with spatial frequency patterns onto tissue allowing for separation of optical properties. The decoupling of optical absorption from scattering enables the use of Beer-Lambert Law to extract chromophores at varied depths from projected wavelengths such as oxy/deoxyhemoglobin, lipids, and water content.[31,32] Clinical applications of SFDI include: 1) burn assessment[33,34], 2) mapping skin cancer[35], 3) assessing tissue perfusion in diabetics[9] 4) vascular assessment[36], and 5) surgical guidance.[37] Previously SFDI imaging studies correlated the oxygen saturation in the papillary and reticular hemoglobin content with healing rates in diabetic ulcers.[9] Further investigation into perfusion mechanics in diabetic and neuropathic disease may allow earlier detection of disease progression.

In this pilot study, we use SFDI to spatially quantify perfusion dynamics of the foot in three postural conditions (supine, elevated limb, reclining) to explore altered tissue perfusion unique to diabetes and neuropathy. Common plantar regions of the foot for ulcer formation include the 1st, 3rd, 5th metatarsal heads and heel. The 3rd metatarsal head and whole foot median values are presented to reduce potential optical edge effects. A quantified difference in perfusion related to position was expected with both median foot values and the 3rd metatarsal head region. We hypothesize quantifying perfusion response of the planar region under various postural conditions may allow for earlier detection of neuropathic damage through early detection of vascular insufficiencies.

Methods

This clinical pilot study was approved by the institutional review board of The University of Maine. Regional oxygen saturation (StO2), superficial papillary plexus microvasculature (HbT1), and reticular deep plexus (HbT2) values are reported for 19 total participants, 8 young-healthy, 4 old-healthy, 4 diabetics, and 3 neuropathy patients. Study participants were grouped into Young (< 50) and Old (50≥) years old and were further classified as healthy, diabetic, or neuropathic patients based on self-reported questionnaire of previous physician diagnosis. All diabetic and neuropathic participants were above 50 years old. An equal distribution of sex was accomplished among all participant groups. One foot of each participant was selected for imaging using the following criteria: does not have calluses within the third metatarsal head region, no prior ulcer formation, and no discoloration of the foot. All study participants had not vigorously exercised within 30 minutes prior to beginning the study. The soles of participants' feet were imaged using Clarifi®, a commercial SFDI device manufactured by Modulim. SFDI relies on optical scattering and absorption of tissue content at several wavelengths with a varied frequency to estimate chromophore concentration.[31] The Clarifi® spatially projects sequential wavelengths and captures images of patterned and planar light (five visible and near infrared wavelengths, [470-850 nm]). The Clarifi® system processes the images to provide spatial maps of tissue perfusion of the dermis and epidermis to a thickness of 5mm enabling quantification of the dermal layers.[19,38,39]

Prior to each study participant trial, the Clarifi® was calibrated as recommended by the manufacturer. The calibration sequence was performed with all the lights off in the room and the instrument response was verified using a calibration phantom with known optical properties. The study participant observed the calibration process as part of the study onboarding. Once the system was calibrated, the participants removed their socks and laid supine on a medical exam table with the lights turned off. After 10 minutes of laying supine optical data was collected and leg position elevated 20 degrees relative to heart, following 10 minutes of foot elevation the foot was lowered 'reclined' 20 degrees below heart level. (Fig. 24) SFDI images were acquired in 5-minute intervals in each of the positional maneuvers. To maximize accuracy, the distance calibration point was focused on the mid pad (roughly 3rd metatarsal head) of the foot for all data. An overview of testing is provided below (Fig. 24**)** indicating postural changes and data labelling. Each position was held for a total of 10 minutes with the intent of achieving homeostasis during which data sets were acquired every 5 minutes as an adjunct for short term physiologic response. At each 5- and 10-minute interval a 10 second SFDI imaging sequence was acquired to calculate tissue perfusion metrics

(StO2, HbT1, HbT2). During each data collection the mid pad of the foot's temperature was collected with a commercial wireless thermometer (Range: 34-40C°, ±0.1). The temperature of the testing environment was variable (23 C°± 4). Several tests were done to isolate the most statistically relevant data with an alpha of 0.05, 2 tailed heteroscedastic T Tests, ANOVA single factor, and Mann Whitney U critical value test. ANOVA single factor and Mann Whitney U tests were utilized to handle small sample size data. All data points that are statistically significant (passed all three previously mentioned tests) with respect to one another in figures will be indicated as * for $p<0.05$.

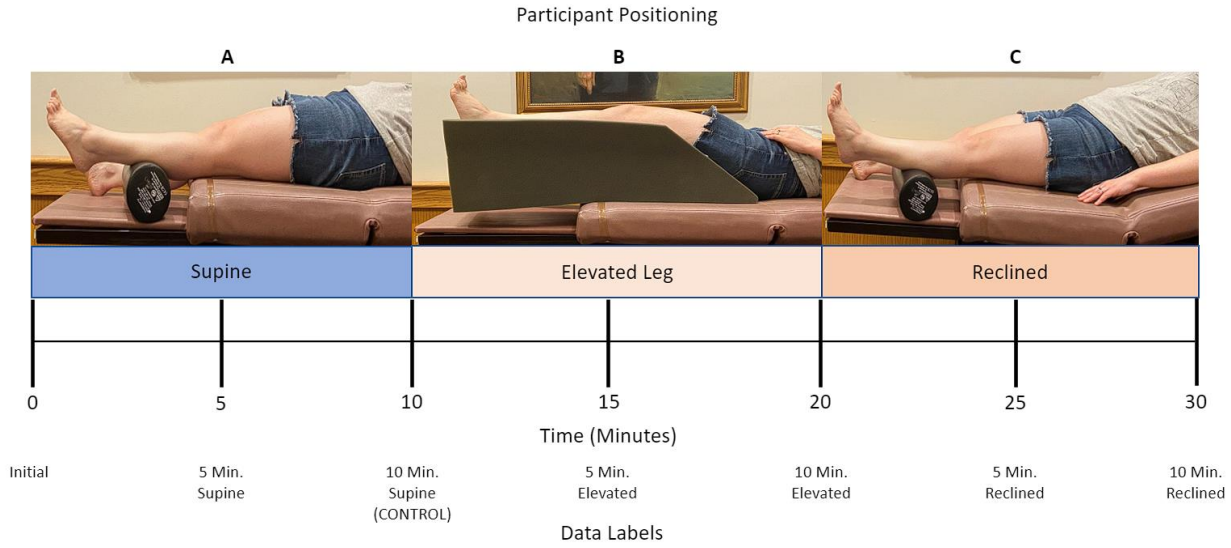

Figure 24: Participant positions during data collection with overview and data labels. **A)** Supine with foot approximating heart height, **B**) Elevated pad of the foot at approximately 20-degrees relative to the table, **C**) Reclined foot with table back elevated approximately 20-degree angle relative to leg.

Results

The total hemoglobin (tHb) in the elevated position was consistently reduced in all groups where tHb is the sum of HbT1 and HbT2. (Fig. 25 A) In all groups, the reduction in tHb was often due to the lower blood net as indicated by the average decrease in the HbT2/HbT1 ratio when the participants' feet were elevated. (Fig. 25 B**)** All participants experienced approximately a 50% reduction in the median HbT1 and HbT2 during the transition from supine to elevated foot position. When reclined a return to the 10-minute supine control value is seen across all groups and in several instances an increase of blood relative to control. Large standard deviation within participant

groups indicates the natural variation of tissue within participant groups. Healthy and young participants had the smallest perturbation of hemoglobin from control due to elevation of the foot amongst all groups (Fig. 25 C, D, Table 3).

Figure 25: Average change in median foot perfusion metrics relative to supine control values.

Region of Interest	Metric	Foot Position (10Min)	Healthy-Young	Healthy-Old	Diabetic	Neuropathy
3rd Metatarsal	StO2	Elevated	+5±15%	+10±28%	-8±13%	+2±7%
		Reclined	-3±19%	-8±8%	-8±12%	-10±8%
	HbT1	Elevated	-8±4	-11±4	-11±11	-9±16
		Reclined	+1±10	0±3	+1±8	+6±11
	HbT2	Elevated	-10±23	-15±15	-19±25	-35±30
		Reclined	+11±22	-6±13	+14±11	-6±21
Median Values Whole Foot	StO2	Elevated	+5±12%	-3±24%	-6±9%	-2±10%
		Reclined	+1±13%	-10±9%	-8±6%	-10±8%
	HbT1	Elevated	-6±4	-10±2	-8±7	-12±10
		Reclined	-2±4	+1±1	+2±4	0±8
	HbT2	Elevated	-13±15	-17±14	-20±26	-30±16
		Reclined	+8±12	-1±8	+5±5	0±10
	HbT2/HbT1 Ratio	Elevated	-0.28±0.29	-0.37±0.17	-0.41±0.57	-0.41±0.30
		Reclined	+0.30±0.42	-0.01±0.20	+0.14±0.05	+0.02±0.20

Table 3: Difference in metrics from control dependent on participant position, values are mean of patient group.

Table 4 shows characteristics of various group subjects in addition to overall averages throughout the experimental procedure. All data is shown as mean±standard deviation. On average, neuropathy participants had much higher HbT2 (deep blood net hemoglobin), in both 3rd metatarsal values and median of whole foot values, relative to other participants groups. Inversely, healthy-old participants had the lowest HbT2 averages throughout in both metrics,

however with large variability in data. HbT2/HbT1 ratio on average was higher in neuropathy participants and reduced in healthy-old participants.

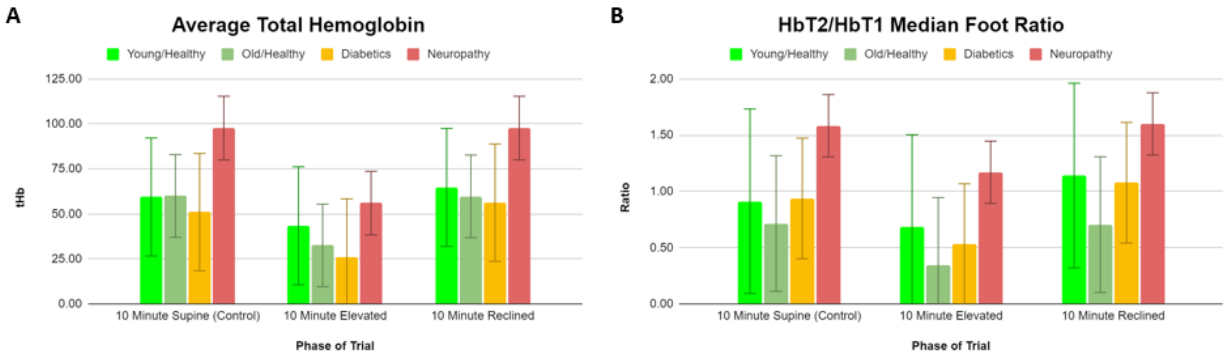

Figure 26: Hemoglobin metrics of all participant groups and positions A) Average total hemoglobin (tHb) for 10-minute positional values by participant groups. B) Ratio of microcirculation hemoglobin to superficial hemoglobin of the whole foot for 10-minute positional values by participant groups.

	Metric	Healthy-Young	Healthy-Old	Diabetic	Neuropathy
Participant Information	Number	8	4	4	3
	Age (years)	30.25±11.6	58.25±6.4	63±3.37	63.3±7.5
	Sex M/F	4/4	2/2	2/2	1/2
3rd Metatarsal Values	StO2	73%±27%	50%±32%	66%±28%	81%±10%
	HbT1	34±10	34±3.7	31±14	38±7.8
	HbT2	30±31	**15±19**	29±26	**65±20***
Median Foot Values	StO2	75%±22%	**57%±24%**	70%±21%	79%±12%
	HbT1	29±8	31±5	27±8	35±5
	HbT2	29±28	20±23	27±20	**53±14****
	HbT2/HbT1 Ratio	0.91±0.82	**0.58±0.66**	0.9±0.46	**1.48±0.28****

Table 4: Data overview of participant characteristics and results, values are overall mean±SD, **bolded** values are considered outliers. * $p<0.05$ relative to healthy-young, ** $p<0.05$ relative to healthy-old

Table 5 shows Pearson correlation coefficient values for experimental groups in altered positions with comparison values taken from 10-minute Supine. Pearson correlations were indicative of predictability of perfusion metrics in altered states such that a high value (0.5-1) indicates high predictability, medium values (0.3-0.49) indicate medium correlation, and low values (0-0.29) indicating low correlation. Negative correlation coefficients such as within the Neuropathy group represent an inverse relationship of resultant position values to supine control. Statistical relevancy of Pearson correlation coefficient calculations is highly sensitive to low sample sizes. This causes many values in the Healthy-Old, Diabetic, and Neuropathy groups to not be statistically relevant. Of note, Neuropathy is the only group with negative correlations throughout the experiment occurring during elevation of the foot. Additionally, high correlation is common in Healthy-Old, Diabetic, and Neuropathy groups in the reclined position with diminished correlation for elevated values.

Region of Interest	Metric	Foot Position (10Min)	Healthy-Young	Healthy-Old	Diabetic	Neuropathy
3rd Metatarsal	StO2	Elevated	0.905*	0.708	0.876	0.908
		Reclined	0.814*	0.985*	0.959*	0.960
	HbT1	Elevated	0.906*	0.859	0.729	**-0.939**
		Reclined	0.486	0.885	0.869	**-0.516**
	HbT2	Elevated	0.664	0.969*	0.509	**-0.452**
		Reclined	0.850*	**0.999***	0.931	0.674
Median Values of Whole Foot	StO2	Elevated	0.952*	0.658	0.879	0.986
		Reclined	0.932*	0.942	0.984*	0.962
	HbT1	Elevated	0.876*	0.848	0.819	**-0.923**
		Reclined	0.901*	0.966*	0.930	0.015
	HbT2	Elevated	0.884*	0.989*	0.603	**-0.028**
		Reclined	0.927*	**0.998***	**0.995***	**0.991**
	HbT2/HbT1 Ratio	Elevated	0.954*	0.990*	0.133	0.617
		Reclined	0.892*	**0.998***	**0.998***	0.863

Table 5: Overview of Pearson correlation coefficients comparing group supine values to elevated foot and reclined position values. Bolded values are considered notable, * $p<0.05$

Discussion

In this pilot study, we demonstrated a potential medical application of SFDI to detect deviations in hemoglobin dynamics in response to alterations in positional dynamics within participants groups. The study methodology is structured for clinical replication using hospital beds, or stretchers, and the Clarifi® mobile SFDI system. To our knowledge, pre-ulcer SFDI data with varying position comparing healthy participant groups to disease status has yet to be completed. Large scale clinical testing may elucidate SFDI as a relevant tool for peripheral neuropathy detection for its ability to quantify superficial perfusion. Foot perfusion metrics have been proven to degrade during disease progression and ultimately lead to ulceration.[10,40,41] Previous studies have presented SFDI methods as a valuable noninvasive tool in quantification of tissue healing and detection of planar foot ulceration.[42]

Previous medical standards for DFU have included elevation of the foot with the intent of increased oxygen saturation of the region and minimizing edema. Superficial perfusion is considered key to wound healing for oxygen and collagen formation. Recent research has questioned the efficacy of foot elevation as a technique to increase perfusion quality within the plantar region of the foot.[2,43,44] Data from this study may indicate further investigation into foot lowering rather than elevating to increase regional perfusion. (Fig. 26) There was minimal change of plantar StO2 to offset for reduced hemoglobin concentration during foot elevation compared to control values. All participant data, irrelevant of group, indicates reduced perfusion in both papillary and reticular circulation during elevation.

Neuropathy participants relative to healthy-old control participants of similar age had substantial differences in certain perfusion metrics including significantly heightened average of HbT2 and subsequently high HbT2/HbT1 ratio. (Table 4) This supports the shunting hypothesis within neuropathic patients whereby a portion of perfusion from the foot bypasses capillaries in favor of deep vessel shunting.[45] Interestingly, superficial capillaries contained roughly equivalent HbT1 across all groups as an indication of quality perfusion. Therefore, in neuropathy participants, the presented data indicates a higher volume of blood in deep capillaries may be needed for equivalent superficial capillary perfusion.

Plantar StO2 was stable throughout the trial relative to hemoglobin quantities and position independent. Healthy-old participants had a low StO2 relative to other participant groups (Table 4) with an upward trend of StO2 in diabetic and neuropathic participant values. The phenomenon of increasing StO2 with disease state may in part be explained by reduced capillary perfusion, instead favoring papillary shunting, causing oxygen dissociation from hemoglobin to be reduced.[41] Healthy-old participant low StO2 values may be partially explained due to a decreased HbT2/HbT1 ratio, whereby less reticular hemoglobin was present relative to papillary hemoglobin. StO2 data presented is supportive of previous findings showing an increase in StO2 for diabetic patients relative to healthy patients of same age.[36,41]

Given the scope of this pilot study, data collection of in-hospital patients was unavailable instead relying on volunteers for participation. Due to high variation of intra-group values and sample size minimal statistical significance between groups could be established. The presented study is novel in presenting quantified positional correlated perfusion metrics utilizing SFDI. From the presented data SFDI was shown to have potential as a rapid, large field of view, and safe technique to quantify regional perfusion. In future iterations of this study a secondary StO2 monitoring device such as a pulse oximeter is recommended as a systemic reference to plantar StO2. Additionally, quantifying and ensuring stable blood pressure would reduce concern for potential factors outside of positional effects. Rapid sequential image collection has sensitivity to movement between images which may incur error. Careful consideration was used in this study to ask participants to minimize movements during each data collection.

Conclusion

To our knowledge this is the first study to quantify perfusion metrics across age and disease status groups with varying positions utilizing SFDI. Our data indicates a significant increase of reticular hemoglobin within neuropathic patients, a universal reduction in perfusion quality during elevation of extremity, and a trend of increasing plantar StO2 with disease state in older adults. Given the scale of the study statistical significance was difficult to ascertain as such, a clinical trial focusing on collecting a large data set of healthy and disease state perfusion metrics with respect to position is recommended. Additional metrics recommended for future work include an independent StO2 monitor on an upper extremity, temperature monitoring of the tested regions of the foot, larger cohort size, and scattering coefficient data to test for structural changes in regions of interest.

Chapter 3 References

1. Centers for Disease Control and Prevention. National Diabetes Statistics Report website. https://www.cdc.gov/diabetes/data/statistics-report/index.html. Accessed 7/13/22.

2. Saeedi, P., Petersohn, I., Salpea, P., et al. (2019). Global and regional diabetes prevalence estimates for 2019 and projections for 2030 and 2045: Results from the International Diabetes Federation Diabetes Atlas, 9th edition. *Diabetes research and clinical practice*, *157*, 107843. https://doi.org/10.1016/j.diabres.2019.107843

3. Faselis C, Katsimardou A, Imprialos K, Deligkaris P, Kallistratos M, Dimitriadis K. Microvascular Complications of Type 2 Diabetes Mellitus. Curr Vasc Pharmacol (2020) 18(2):117–24. doi: 10.2174/1570161117666190502103733

4. Ziegler, D., Papanas, N., Schnell, O., et al. (2021). Current concepts in the management of diabetic polyneuropathy. *Journal of Diabetes Investigation*, *12*(4), 464–475. https://doi.org/10.1111/jdi.13401

5. Vincent, A. M., Callaghan, B. C., Smith, A. L., & Feldman, E. L. (2011). Diabetic neuropathy: cellular mechanisms as therapeutic targets. *Nature Reviews Neurology*, *7*(10), 573–583. https://doi.org/10.1038/nrneurol.2011.137

6. The, W. I. S., Peripheral, I. O. F., & In, A. D. (2003). Epidemiology and Impact of Peripheral Arterial Disease in People with Diabetes. *Diabetes*, *26*(12), 3333–3341. http://www.ncbi.nlm.nih.gov/pubmed/14633825

7. Bridges, R. M., & Deitch, E. A. (1994). Diabetic foot infections: Pathophysiology and treatment. *Surgical Clinics of North America*, *74*(3), 537–555. https://doi.org/10.1016/s0039-6109(16)46328-0

8. Balasubramanian, G. V., Chockalingam, N., & Naemi, R. (2021). The Role of Cutaneous Microcirculatory Responses in Tissue Injury, Inflammation and Repair at the Foot in Diabetes. *Frontiers in Bioengineering and Biotechnology*, *9*(September), 1–11. https://doi.org/10.3389/fbioe.2021.732753

9. Li, Y., Guo, M., Qian, X., et al. (2020). Single snapshot spatial frequency domain imaging for risk stratification of diabetes and diabetic foot. *Biomedical Optics Express*, *11*(8), 4471. https://doi.org/10.1364/boe.394929

10. Yafi, A., Muakkassa, F. K., Pasupneti, T., et al. (2017). Quantitative skin assessment using spatial frequency domain imaging (SFDI) in patients with or at high risk for pressure ulcers. *Lasers in Surgery and Medicine*, *49*(9), 827–834. https://doi.org/10.1002/lsm.22692

11. Bondar, A., Popa, A., Papanas, N., et al. (2021). Diabetic neuropathy: A narrative review of risk factors, classification, screening and current pathogenic treatment options (Review). *Experimental and Therapeutic Medicine*, *22*(1). https://doi.org/10.3892/etm.2021.10122

12. Giacco, F., & Brownlee, M. (2010). Oxidative stress and diabetic complications. In *Circulation Research* (Vol. 107, Issue 9, pp. 1058–1070). https://doi.org/10.1161/CIRCRESAHA.110.223545

13. Kawasaki, T., Uemura, T., Matsuo, K., et al. (2013). The effect of different positions on lower limbs skin perfusion pressure. In *Indian Journal of Plastic Surgery* (Vol. 46, Issue 3, pp. 508–512). https://doi.org/10.4103/0970-0358.121995

14. O'Brien, T. D. (2020). Impaired dermal microvascular reactivity and implications for diabetic wound formation and healing: an evidence review. *Journal of Wound Care*, *29*(Sup9), S21–S28. https://doi.org/10.12968/jowc.2020.29.Sup9.S21

15. Schie, C. H. M. Van. (2005). *A Review of the Biomechanics of the Diabetic Foot*. *4*(3), 160–170. https://doi.org/10.1177/1534734605280587

16. Yagihashi, S., Mizukami, H., & Sugimoto, K. (2011). *Mechanism of diabetic neuropathy : Where are we now and where to go ? 2*(1), 18–32. https://doi.org/10.1111/j.2040-1124.2010.00070.x

17. Brownrigg, J. R. W., Hinchliffe, R. J., Apelqvist, J., et al. (2016). Performance of prognostic markers in the prediction of wound healing or amputation among patients with foot ulcers in diabetes: a systematic review. *Diabetes/Metabolism Research and Reviews*, *32*(30), 128–135. https://doi.org/10.1002/dmrr.2704

18. Iwase, M., Imoto, H., Murata, A., et al. (2007). Altered postural regulation of foot skin oxygenation and blood flow in patients with type 2 diabetes mellitus. *Experimental and Clinical Endocrinology and Diabetes*, *115*(7), 444–447. https://doi.org/10.1055/s-2007-960499

19. Yu, Y. (2021). Gold Standard for Diagnosis of DPN. *Frontiers in Endocrinology*, *12*(October), 1–6. https://doi.org/10.3389/fendo.2021.719356

20. McIllhatton, A., Lanting, S., Lambkin, D., Leigh, L., Casey, S., & Chuter, V. (2021). Reliability of recommended non-invasive chairside screening tests for diabetes-related peripheral neuropathy: A systematic review with meta-analyses. *BMJ Open Diabetes Research and Care*, *9*(2). https://doi.org/10.1136/bmjdrc-2021-002528

21. Ziegler, D., Papanas, N., Schnell, O., et al. (2021). Current concepts in the management of diabetic polyneuropathy. *Journal of Diabetes Investigation*, *12*(4), 464–475. https://doi.org/10.1111/jdi.13401

22. Sandby-Møller, J., Poulsen, T., & Wulf, H. C. (2003). Epidermal Thickness at Different Body Sites: Relationship to Age, Gender, Pigmentation, Blood Content, Skin Type and Smoking Habits. *Acta Dermato-Venereologica*, *83*(6), 410–413. https://doi.org/10.1080/00015550310015419

23. Hoi, J. W., Kim, H. K., Fong, C. J., Zweck, L., & Hielscher, A. H. (2018). Non-contact dynamic diffuse optical tomography imaging system for evaluating lower extremity vasculature. *Biomedical Optics Express*, *9*(11), 5597. https://doi.org/10.1364/boe.9.005597

24. Zharkikh, E., Dremin, V., Zherebtsov, E., Dunaev, A., & Meglinski, I. (2020). Biophotonics methods for functional monitoring of complications of diabetes mellitus. *Journal of Biophotonics*, *13*(10), 1–20. https://doi.org/10.1002/jbio.202000203

25. Mennes, O. A., Van Netten, J. J., Van Baal, J. G., & Steenbergen, W. (2019). Assessment of microcirculation in the diabetic foot with laser speckle contrast imaging. *Physiological Measurement*, *40*(6). https://doi.org/10.1088/1361-6579/ab2058

26. Lu, G., & Fei, B. (2014). Medical hyperspectral imaging: a review. *Journal of Biomedical Optics*, *19*(1), 010901. https://doi.org/10.1117/1.jbo.19.1.010901

27. Applegate, M. B., Istfan, R. E., Spink, S., Tank, A., & Roblyer, D. (2020). Recent advances in high speed diffuse optical imaging in biomedicine. *APL Photonics*, *5*(4). https://doi.org/10.1063/1.5139647

28. Rajan, V., Varghese, B., van Leeuwen, T. G., & Steenbergen, W. (2009). Review of methodological developments in laser Doppler flowmetry. In *Lasers in Medical Science* (Vol. 24, Issue 2, pp. 269–283). https://doi.org/10.1007/s10103-007-0524-0

29. Heeman, W., Steenbergen, W., van Dam, G. M., & Boerma, E. C. (2019). Clinical applications of laser speckle contrast imaging: a review. *Journal of Biomedical Optics*, *24*(08), 1. https://doi.org/10.1117/1.jbo.24.8.080901

30. Torabzadeh, M., Stockton, P. A., Kennedy, G. T., et al. (2019). Hyperspectral imaging in the spatial frequency domain with a supercontinuum source. *Journal of Biomedical Optics*, *24*(07), 1. https://doi.org/10.1117/1.jbo.24.7.071614

31. Gioux, S., Mazhar, A., & Cuccia, D. J. (2019). Spatial frequency domain imaging in 2019: principles, applications, and perspectives. *Journal of Biomedical Optics*, *24*(07), 1. https://doi.org/10.1117/1.JBO.24.7.071613

32. Mazhar, A., Dell, S., Cuccia, D. J., Gioux, S., et al. (2010). Wavelength optimization for rapid chromophore mapping using spatial frequency domain imaging. *Journal of Biomedical Optics*, *15*(6), 61716. https://doi.org/10.1117/1.3523373

33. Mazhar, A., Saggese, S., Pollins, A. C., Cardwell, N. L., Nanney, L., & Cuccia, D. J. (2014). Noncontact imaging of burn depth and extent in a porcine model using spatial frequency domain imaging. *Journal of Biomedical Optics*, *19*(8), 086019. https://doi.org/10.1117/1.JBO.19.8.086019

34. Burmeister, D. M., Ponticorvo, A., Yang, B., et al. (2015). Utility of spatial frequency domain imaging (SFDI) and laser speckle imaging (LSI) to non-invasively diagnose burn depth in a porcine model. *Burns*, *41*(6), 1242–1252. https://doi.org/10.1016/j.burns.2015.03.001

35. Rohrbach, D. J., Muffoletto, D., Huihui, J., et al. (2014). Preoperative Mapping of Nonmelanoma Skin Cancer Using Spatial Frequency Domain and Ultrasound Imaging. *Academic Radiology*, *21*(2), 263–270. https://doi.org/10.1016/j.acra.2013.11.013

36. Weinkauf, C., Mazhar, A., Vaishnav, K., Hamadani, A. A., Cuccia, D. J., & Armstrong, D. G. (2019). Near-instant noninvasive optical imaging of tissue perfusion for vascular assessment. *Journal of Vascular Surgery*, *69*(2), 555–562. https://doi.org/10.1016/j.jvs.2018.06.202

37. Nguyen, J. T., Lin, S. J., Tobias, A. M., et al. (2013). A novel pilot study using spatial frequency domain imaging to assess oxygenation of perforator flaps during reconstructive breast surgery. *Annals of Plastic Surgery*, *71*(3), 308–315. https://doi.org/10.1097/SAP.0b013e31828b02fb

38. Chao, C. Y. L., Zheng, Y. P., & Cheing, G. L. Y. (2011). Epidermal Thickness and Biomechanical Properties of Plantar Tissues in Diabetic Foot. *Ultrasound in Medicine and Biology*, *37*(7), 1029–1038. https://doi.org/10.1016/j.ultrasmedbio.2011.04.004

39. Murphy, G. A., Singh-Moon, R. P., Mazhar, A., Cuccia, D. J., Rowe, V. L., & Armstrong, D. G. (2020). Quantifying dermal microcirculatory changes of neuropathic and neuroischemic diabetic foot ulcers using spatial frequency domain imaging: A shade of things to come? *BMJ Open Diabetes Research and Care*, *8*(2), 1–8. https://doi.org/10.1136/bmjdrc-2020-001815

40. Weingarten, M. S., Samuels, J. A., Neidrauer, M., et al. (2012). Diffuse near-infrared spectroscopy prediction of healing in diabetic foot ulcers: A human study and cost analysis. *Wound Repair and Regeneration*, *20*(6), 911–917. https://doi.org/10.1111/j.1524-475X.2012.00843.x

41. Lee, S., Mey, L., Szymanska, A. F., et al. (2020). SFDI biomarkers provide a quantitative ulcer risk metric and can be used to predict diabetic foot ulcer onset. *Journal of Diabetes and Its Complications*, *34*(9), 107624. https://doi.org/10.1016/j.jdiacomp.2020.107624

42. Weinkauf, C., Mazhar, A., Vaishnav, K., Hamadani, A. A., Cuccia, D. J., & Armstrong, D. G. (2019). Near-instant noninvasive optical imaging of tissue perfusion for vascular assessment. *Journal of Vascular Surgery*, *69*(2), 555–562. https://doi.org/10.1016/j.jvs.2018.06.202

43. Han, S.-K. (2017). Increasing Tissue Oxygenation for Diabetic Wound Healing. *Journal of Wound Management and Research*, *13*(1), 2–7. https://doi.org/10.22467/jwmr.2017.00080

44. Park, D. J., Han, S. K., & Kim, W. K. (2010). Is the foot elevation the optimal position for wound healing of a diabetic foot? *Journal of Plastic, Reconstructive and Aesthetic Surgery*, *63*(3), 561–564. https://doi.org/10.1016/j.bjps.2008.11.042

45. Vouillarmet, J., Josset-Lamaugarny, A., Michon, P., et al. (2019). Neurovascular response to pressure in patients with diabetic foot ulcer. *Diabetes*, *68*(4), 832–836. https://doi.org/10.2337/db18-0694

REFERENCES

Pogue, B. W. (2018, January 22). Optics of Medical Imaging. Retrieved May 14, 2022, from https://spie.org/news/spie-professional-magazine-archive/2018-january/optics-of-medical-imaging?SSO=1

Ponticorvo, A., Burmeister, D. M., Yang, B., Choi, B., Christy, R. J., & Durkin, A. J. (2014). Quantitative assessment of graded burn wounds in a porcine model using spatial frequency domain imaging (SFDI) and laser speckle imaging (LSI). *Biomedical Optics Express*, *5*(10), 3467. https://doi.org/10.1364/boe.5.003467

Mazhar, A., Saggese, S., Pollins, A. C., Cardwell, N. L., Nanney, L., & Cuccia, D. J. (2014). Noncontact imaging of burn depth and extent in a porcine model using spatial frequency domain imaging. *Journal of Biomedical Optics*, *19*(8), 086019. https://doi.org/10.1117/1.JBO.19.8.086019

Weinkauf, C., Mazhar, A., Vaishnav, K., Hamadani, A. A., Cuccia, D. J., & Armstrong, D. G. (2019). Near-instant noninvasive optical imaging of tissue perfusion for vascular assessment. *Journal of Vascular Surgery*, *69*(2), 555–562. https://doi.org/10.1016/j.jvs.2018.06.202

Leyba, K., Vasudevan, S., O'Sullivan, T., & Goergen, C. (2020). *Spatial frequency domain imaging of hemodynamic parameters in a murine model of hindlimb ischemia*. *February*, 11. https://doi.org/10.1117/12.2541944

Li, Y., Guo, M., Qian, X., Lin, W., Zheng, Y., Yu, K., Zeng, B., Xu, Z., Zheng, C., & Xu, M. (2020). Single snapshot spatial frequency domain imaging for risk stratification of diabetes and diabetic foot. *Biomedical Optics Express*, *11*(8), 4471. https://doi.org/10.1364/boe.394929

Rohrbach, D. J., Muffoletto, D., Huihui, J., Saager, R., Keymel, K., Paquette, A., Morgan, J., Zeitouni, N., & Sunar, U. (2014). Preoperative Mapping of Nonmelanoma Skin Cancer Using Spatial Frequency Domain and Ultrasound Imaging. *Academic Radiology*, *21*(2), 263–270. https://doi.org/10.1016/j.acra.2013.11.013

Laughney, A. M., Krishnaswamy, V., Rice, T. B., Cuccia, D. J., Barth, R. J., Tromberg, B. J., Paulsen, K. D., Pogue, B. W., & Wells, W. A. (2013). System analysis of spatial frequency domain imaging for quantitative mapping of surgically resected breast tissues. *Journal of Biomedical Optics*, *18*(3), 036012. https://doi.org/10.1117/1.jbo.18.3.036012

Hayakawa, C. K., Karrobi, K., Pera, V., Roblyer, D., & Venugopalan, V. (2018). Optical sampling depth in the spatial frequency domain. *Journal of Biomedical Optics*, *24*(07), 1. https://doi.org/10.1117/1.jbo.24.7.071603

Gioux, S., Mazhar, A., & Cuccia, D. J. (2019). Spatial frequency domain imaging in 2019: principles, applications, and perspectives. *Journal of Biomedical Optics*, *24*(07), 1. https://doi.org/10.1117/1.JBO.24.7.071613

Lepelaars, E. S. A. M. (1996). Electromagnetic pulse distortion in living tissue. *Medical and Biological Engineering and Computing*, *34*(3), 213–220. https://doi.org/10.1007/BF02520076

Mazhar, A., Dell, S., Cuccia, D. J., Gioux, S., Durkin, A. J., Frangioni, J. V., & Tromberg, B. J. (2010). Wavelength optimization for rapid chromophore mapping using spatial frequency domain imaging. *Journal of Biomedical Optics*, *15*(6), 061716. https://doi.org/10.1117/1.3523373

Erfanzadeh, M., Nandy, S., Kumavor, P. D., & Zhu, Q. (2018). Low-cost compact multispectral spatial frequency domain imaging prototype for tissue characterization. *Biomedical Optics Express*, *9*(11), 5503. https://doi.org/10.1364/boe.9.005503

Bodenschatz, N., Brandes, A., Liemert, A., & Kienle, A. (2014). Sources of errors in spatial frequency domain imaging of scattering media. *Journal of Biomedical Optics*, *19*(7), 071405. https://doi.org/10.1117/1.jbo.19.7.071405

Tabassum, S., Pera, V., Greening, G., Muldoon, T. J., & Roblyer, D. (2018). Two-layer inverse model for improved longitudinal preclinical tumor imaging in the spatial frequency domain. *Journal of Biomedical Optics*, *23*(07), 1. https://doi.org/10.1117/1.jbo.23.7.076011

Neel Joshi, Craig Donner, and Henrik Wann Jensen, "Noninvasive measurement of scattering anisotropy in turbid materials by nonnormal incident illumination," Opt. Lett. 31, 936-938 (2006)

Angelo, J., Vargas, C. R., Lee, B. T., Bigio, I. J., & Gioux, S. (2016). Ultrafast optical property map generation using lookup tables. *Journal of Biomedical Optics*, *21*(11), 110501. https://doi.org/10.1117/1.jbo.21.11.110501

Prahl, S. (n.d.). *Optical Absorption of Hemoglobin*. Optical absorption of hemoglobin. Retrieved May 30, 2022, from https://omlc.org/spectra/hemoglobin/

SFDI 101. Open SFDI. (n.d.). Retrieved June 11, 2022, from http://opensfdi.org/sfdi-101/

Lehmann H. Acupuncture in ancient China: how important was it really? J Integr Med. 2013 Jan;11(1):45-53. doi: 10.3736/jintegrmed2013008. PMID: 23464646.

The history of microneedling and Facelifts. MDPen. (2020, June 15). Retrieved April 29, 2022, from https://mdpen.co/the-history-of-microneedling-and-facelifts/

Liebl, H., & Kloth, L. C. (2012). Skin cell proliferation stimulated by microneedles. Journal of the American College of Clinical Wound Specialists, 4(1), 2–6. https://doi.org/10.1016/j.jccw.2012.11.001

Singh, A., & Yadav, S. (2016). Microneedling: Advances and widening horizons. Indian Dermatology Online Journal, 7(4), 244. https://doi.org/10.4103/2229-5178.185468

Cárcamo-Martínez, Á., Mallon, B., Domínguez-Robles, J., Vora, L. K., Anjani, Q. K., & Donnelly, R. F. (2021). Hollow microneedles: A perspective in biomedical applications. International Journal of Pharmaceutics, 599(March). https://doi.org/10.1016/j.ijpharm.2021.120455

Coppola, S., Vespini, V., Nasti, G., & Ferraro, P. (2021). Transmitting Light through Biocompatible and Biodegradable Drug Delivery Micro Needles. *IEEE Journal of Selected Topics in Quantum Electronics*, *27*(5). https://doi.org/10.1109/JSTQE.2021.3057834

Mccrudden, M. T. C., Mcalister, E., Courtenay, A. J., González-Vázquez, P., Raj Singh, T. R., & Donnelly, R. F. (2015). Microneedle applications in improving skin appearance. Experimental Dermatology, 24(8), 561–566. https://doi.org/10.1111/exd.12723

Rosenberry, R., & Nelson, M. D. (2020). Reactive hyperemia: A review of methods, mechanisms, and considerations. *American Journal of Physiology - Regulatory Integrative and Comparative Physiology*, *318*(3), R605–R618. https://doi.org/10.1152/AJPREGU.00339.2019

Samant, P. P., & Prausnitz, M. R. (2018). Mechanisms of sampling interstitial fluid from skin using a microneedle patch. *Proceedings of the National Academy of Sciences of the United States of America*, *115*(18), 4583–4588. https://doi.org/10.1073/pnas.1716772115

Zwanenburg, P. R., Backer, S. F. M., Obdeijn, M. C., Lapid, O., Gans, S. L., & Boermeester, M. A. (2019). A Systematic Review and Meta-Analysis of the Pressure-Induced Vasodilation Phenomenon and Its Role in the

Pathophysiology of Ulcers. *Plastic and Reconstructive Surgery*, *144*(4), 669e-681e. https://doi.org/10.1097/PRS.0000000000006090

Maiti, R., Duan, M., Danby, S. G., Lewis, R., Matcher, S. J., & Carré, M. J. (2020). Morphological parametric mapping of 21 skin sites throughout the body using optical coherence tomography. *Journal of the Mechanical Behavior of Biomedical Materials*, *102*(April 2019). https://doi.org/10.1016/j.jmbbm.2019.103501

Balasubramanian, G. V., Chockalingam, N., & Naemi, R. (2021). The Role of Cutaneous Microcirculatory Responses in Tissue Injury, Inflammation and Repair at the Foot in Diabetes. *Frontiers in Bioengineering and Biotechnology*, *9*(September), 1–11. https://doi.org/10.3389/fbioe.2021.732753

Kolarsick, P., Kolarsick, M.A., & Goodwin, C. (2011). Anatomy and Physiology of the Skin. *Journal of the Dermatology Nurses' Association, 3*, 203-213.

Centers for Disease Control and Prevention. National Diabetes Statistics Report website. https://www.cdc.gov/diabetes/data/statistics-report/index.html. Accessed 7/13/22.

Saeedi, P., Petersohn, I., Salpea, P., et al. (2019). Global and regional diabetes prevalence estimates for 2019 and projections for 2030 and 2045: Results from the International Diabetes Federation Diabetes Atlas, 9th edition. *Diabetes research and clinical practice*, *157*, 107843. https://doi.org/10.1016/j.diabres.2019.107843

Faselis C, Katsimardou A, Imprialos K, Deligkaris P, Kallistratos M, Dimitriadis K. Microvascular Complications of Type 2 Diabetes Mellitus. Curr Vasc Pharmacol (2020) 18(2):117–24. doi: 10.2174/1570161117666190502103733

Ziegler, D., Papanas, N., Schnell, O., et al. (2021). Current concepts in the management of diabetic polyneuropathy. *Journal of Diabetes Investigation*, *12*(4), 464–475. https://doi.org/10.1111/jdi.13401

Vincent, A. M., Callaghan, B. C., Smith, A. L., & Feldman, E. L. (2011). Diabetic neuropathy: cellular mechanisms as therapeutic targets. *Nature Reviews Neurology*, *7*(10), 573–583. https://doi.org/10.1038/nrneurol.2011.137

The, W. I. S., Peripheral, I. O. F., & In, A. D. (2003). Epidemiology and Impact of Peripheral Arterial Disease in People with Diabetes. *Diabetes*, *26*(12), 3333–3341. http://www.ncbi.nlm.nih.gov/pubmed/14633825

Bridges, R. M., & Deitch, E. A. (1994). Diabetic foot infections: Pathophysiology and treatment. *Surgical Clinics of North America*, *74*(3), 537–555. https://doi.org/10.1016/s0039-6109(16)46328-0

Balasubramanian, G. V., Chockalingam, N., & Naemi, R. (2021). The Role of Cutaneous Microcirculatory Responses in Tissue Injury, Inflammation and Repair at the Foot in Diabetes. *Frontiers in Bioengineering and Biotechnology*, *9*(September), 1–11. https://doi.org/10.3389/fbioe.2021.732753

Li, Y., Guo, M., Qian, X., et al. (2020). Single snapshot spatial frequency domain imaging for risk stratification of diabetes and diabetic foot. *Biomedical Optics Express*, *11*(8), 4471. https://doi.org/10.1364/boe.394929

Yafi, A., Muakkassa, F. K., Pasupneti, T., et al. (2017). Quantitative skin assessment using spatial frequency domain imaging (SFDI) in patients with or at high risk for pressure ulcers. *Lasers in Surgery and Medicine*, *49*(9), 827–834. https://doi.org/10.1002/lsm.22692

Bondar, A., Popa, A., Papanas, N., et al. (2021). Diabetic neuropathy: A narrative review of risk factors, classification, screening and current pathogenic treatment options (Review). *Experimental and Therapeutic Medicine*, *22*(1). https://doi.org/10.3892/etm.2021.10122

Giacco, F., & Brownlee, M. (2010). Oxidative stress and diabetic complications. In *Circulation Research* (Vol. 107, Issue 9, pp. 1058–1070). https://doi.org/10.1161/CIRCRESAHA.110.223545

Kawasaki, T., Uemura, T., Matsuo, K., et al. (2013). The effect of different positions on lower limbs skin perfusion pressure. In *Indian Journal of Plastic Surgery* (Vol. 46, Issue 3, pp. 508–512). https://doi.org/10.4103/0970-0358.121995

O'Brien, T. D. (2020). Impaired dermal microvascular reactivity and implications for diabetic wound formation and healing: an evidence review. *Journal of Wound Care*, *29*(Sup9), S21–S28. https://doi.org/10.12968/jowc.2020.29.Sup9.S21

Schie, C. H. M. Van. (2005). *A Review of the Biomechanics of the Diabetic Foot*. *4*(3), 160–170. https://doi.org/10.1177/1534734605280587

Yagihashi, S., Mizukami, H., & Sugimoto, K. (2011). *Mechanism of diabetic neuropathy : Where are we now and where to go ? 2*(1), 18–32. https://doi.org/10.1111/j.2040-1124.2010.00070.x

Brownrigg, J. R. W., Hinchliffe, R. J., Apelqvist, J., et al. (2016). Performance of prognostic markers in the prediction of wound healing or amputation among patients with foot ulcers in diabetes: a systematic review. *Diabetes/Metabolism Research and Reviews*, *32*(30), 128–135. https://doi.org/10.1002/dmrr.2704

Iwase, M., Imoto, H., Murata, A., et al. (2007). Altered postural regulation of foot skin oxygenation and blood flow in patients with type 2 diabetes mellitus. *Experimental and Clinical Endocrinology and Diabetes*, *115*(7), 444–447. https://doi.org/10.1055/s-2007-960499

Yu, Y. (2021). Gold Standard for Diagnosis of DPN. *Frontiers in Endocrinology*, *12*(October), 1–6. https://doi.org/10.3389/fendo.2021.719356

McIllhatton, A., Lanting, S., Lambkin, D., Leigh, L., Casey, S., & Chuter, V. (2021). Reliability of recommended non-invasive chairside screening tests for diabetes-related peripheral neuropathy: A systematic review with meta-analyses. *BMJ Open Diabetes Research and Care*, *9*(2). https://doi.org/10.1136/bmjdrc-2021-002528

Ziegler, D., Papanas, N., Schnell, O., et al. (2021). Current concepts in the management of diabetic polyneuropathy. *Journal of Diabetes Investigation*, *12*(4), 464–475. https://doi.org/10.1111/jdi.13401

Sandby-Møller, J., Poulsen, T., & Wulf, H. C. (2003). Epidermal Thickness at Different Body Sites: Relationship to Age, Gender, Pigmentation, Blood Content, Skin Type and Smoking Habits. *Acta Dermato-Venereologica*, *83*(6), 410–413. https://doi.org/10.1080/00015550310015419

Hoi, J. W., Kim, H. K., Fong, C. J., Zweck, L., & Hielscher, A. H. (2018). Non-contact dynamic diffuse optical tomography imaging system for evaluating lower extremity vasculature. *Biomedical Optics Express*, *9*(11), 5597. https://doi.org/10.1364/boe.9.005597

Zharkikh, E., Dremin, V., Zherebtsov, E., Dunaev, A., & Meglinski, I. (2020). Biophotonics methods for functional monitoring of complications of diabetes mellitus. *Journal of Biophotonics*, *13*(10), 1–20. https://doi.org/10.1002/jbio.202000203

Mennes, O. A., Van Netten, J. J., Van Baal, J. G., & Steenbergen, W. (2019). Assessment of microcirculation in the diabetic foot with laser speckle contrast imaging. *Physiological Measurement*, *40*(6). https://doi.org/10.1088/1361-6579/ab2058

Lu, G., & Fei, B. (2014). Medical hyperspectral imaging: a review. *Journal of Biomedical Optics*, *19*(1), 010901. https://doi.org/10.1117/1.jbo.19.1.010901

Applegate, M. B., Istfan, R. E., Spink, S., Tank, A., & Roblyer, D. (2020). Recent advances in high speed diffuse optical imaging in biomedicine. *APL Photonics*, *5*(4). https://doi.org/10.1063/1.5139647

Rajan, V., Varghese, B., van Leeuwen, T. G., & Steenbergen, W. (2009). Review of methodological developments in laser Doppler flowmetry. In *Lasers in Medical Science* (Vol. 24, Issue 2, pp. 269–283). https://doi.org/10.1007/s10103-007-0524-0

Heeman, W., Steenbergen, W., van Dam, G. M., & Boerma, E. C. (2019). Clinical applications of laser speckle contrast imaging: a review. *Journal of Biomedical Optics*, *24*(08), 1. https://doi.org/10.1117/1.jbo.24.8.080901

Torabzadeh, M., Stockton, P. A., Kennedy, G. T., et al. (2019). Hyperspectral imaging in the spatial frequency domain with a supercontinuum source. *Journal of Biomedical Optics*, *24*(07), 1. https://doi.org/10.1117/1.jbo.24.7.071614

Gioux, S., Mazhar, A., & Cuccia, D. J. (2019). Spatial frequency domain imaging in 2019: principles, applications, and perspectives. *Journal of Biomedical Optics*, *24*(07), 1. https://doi.org/10.1117/1.JBO.24.7.071613

Mazhar, A., Dell, S., Cuccia, D. J., Gioux, S., et al. (2010). Wavelength optimization for rapid chromophore mapping using spatial frequency domain imaging. *Journal of Biomedical Optics*, *15*(6), 61716. https://doi.org/10.1117/1.3523373

Mazhar, A., Saggese, S., Pollins, A. C., Cardwell, N. L., Nanney, L., & Cuccia, D. J. (2014). Noncontact imaging of burn depth and extent in a porcine model using spatial frequency domain imaging. *Journal of Biomedical Optics*, *19*(8), 086019. https://doi.org/10.1117/1.JBO.19.8.086019

Burmeister, D. M., Ponticorvo, A., Yang, B., et al. (2015). Utility of spatial frequency domain imaging (SFDI) and laser speckle imaging (LSI) to non-invasively diagnose burn depth in a porcine model. *Burns*, *41*(6), 1242–1252. https://doi.org/10.1016/j.burns.2015.03.001

Rohrbach, D. J., Muffoletto, D., Huihui, J., et al. (2014). Preoperative Mapping of Nonmelanoma Skin Cancer Using Spatial Frequency Domain and Ultrasound Imaging. *Academic Radiology*, *21*(2), 263–270. https://doi.org/10.1016/j.acra.2013.11.013

Weinkauf, C., Mazhar, A., Vaishnav, K., Hamadani, A. A., Cuccia, D. J., & Armstrong, D. G. (2019). Near-instant noninvasive optical imaging of tissue perfusion for vascular assessment. *Journal of Vascular Surgery*, *69*(2), 555–562. https://doi.org/10.1016/j.jvs.2018.06.202

Nguyen, J. T., Lin, S. J., Tobias, A. M., et al. (2013). A novel pilot study using spatial frequency domain imaging to assess oxygenation of perforator flaps during reconstructive breast surgery. *Annals of Plastic Surgery*, *71*(3), 308–315. https://doi.org/10.1097/SAP.0b013e31828b02fb

Chao, C. Y. L., Zheng, Y. P., & Cheing, G. L. Y. (2011). Epidermal Thickness and Biomechanical Properties of Plantar Tissues in Diabetic Foot. *Ultrasound in Medicine and Biology*, *37*(7), 1029–1038. https://doi.org/10.1016/j.ultrasmedbio.2011.04.004

Murphy, G. A., Singh-Moon, R. P., Mazhar, A., Cuccia, D. J., Rowe, V. L., & Armstrong, D. G. (2020). Quantifying dermal microcirculatory changes of neuropathic and neuroischemic diabetic foot ulcers using spatial frequency domain imaging: A shade of things to come? *BMJ Open Diabetes Research and Care*, *8*(2), 1–8. https://doi.org/10.1136/bmjdrc-2020-001815

Weingarten, M. S., Samuels, J. A., Neidrauer, M., et al. (2012). Diffuse near-infrared spectroscopy prediction of healing in diabetic foot ulcers: A human study and cost analysis. *Wound Repair and Regeneration*, *20*(6), 911–917. https://doi.org/10.1111/j.1524-475X.2012.00843.x

Lee, S., Mey, L., Szymanska, A. F., et al. (2020). SFDI biomarkers provide a quantitative ulcer risk metric and can be used to predict diabetic foot ulcer onset. *Journal of Diabetes and Its Complications*, *34*(9), 107624. https://doi.org/10.1016/j.jdiacomp.2020.107624

Weinkauf, C., Mazhar, A., Vaishnav, K., Hamadani, A. A., Cuccia, D. J., & Armstrong, D. G. (2019). Near-instant noninvasive optical imaging of tissue perfusion for vascular assessment. *Journal of Vascular Surgery*, *69*(2), 555–562. https://doi.org/10.1016/j.jvs.2018.06.202

Han, S.-K. (2017). Increasing Tissue Oxygenation for Diabetic Wound Healing. *Journal of Wound Management and Research*, *13*(1), 2–7. https://doi.org/10.22467/jwmr.2017.00080

Park, D. J., Han, S. K., & Kim, W. K. (2010). Is the foot elevation the optimal position for wound healing of a diabetic foot? *Journal of Plastic, Reconstructive and Aesthetic Surgery*, *63*(3), 561–564. https://doi.org/10.1016/j.bjps.2008.11.042

Vouillarmet, J., Josset-Lamaugarny, A., Michon, P., et al. (2019). Neurovascular response to pressure in patients with diabetic foot ulcer. *Diabetes*, *68*(4), 832–836. https://doi.org/10.2337/db18-0694

TRIALS AND TRIBULATIONS

Over the course of the presented thesis several impediments slowed progress and forced change in intended design of experiments. During evaluation of microneedle treatments (Chapter 2) our commercial SFDI system Reflect RS was found to have dysfunction in its 971nm wavelength LED. From our investigation it appeared the 971nm LED had burnt out within the projection case of the system. The use of 971nm light is often key in associating reflected light to tissue water content. Extraction of water content was a primary goal due to the request of approximating interstitial fluid reaction to microneedle use from our collaborator Rosemary Smith. As such the microneedle data presented in this thesis could focus only on the hemoglobin content. However, the feasibility of SFDI to gather microneedle reactivity measurements and interstitial fluid change should still be tested if hardware is available for this purpose.

A second hardware dysfunction related to the Reflect RS occurred when the 851nm wavelength LED was not projecting likely due to internal damage or burning out over time. This hardware concern was found during the first iteration of the presented diabetic study which had originally intended on studying the effect of standing, sitting, and elevating feet. The effect of standing and sitting was to be observed via data collection through a high optical passthrough plexiglass sheet. The Acrylic sheet was procured from ROEHM of America in Sanford, Maine and the physical step design was created by David Crane Carpentry in Houlton, Maine. This would allow full view of the base of the foot while allowing normal walking pressures on the plantar region. The Reflect RS had the capability of imaging the foot through this surface allowing for accurate hemoglobin approximation. When the hardware issue was identified Modulim sent out a secondary device (Clarifi) to utilize in the interim of the Reflect RS's repair. Unfortunately, the Clarifi system was unable to image through the plexiglass surface resulting in high intensity regions reflecting back into the camera and skewing any possible data result. Polarized filtering of the projected light was attempted with the goal of reducing unwanted reflected light which was unsuccessful. Overall, given the correct optical equipment and camera the experiment of quantifying standing, sitting, and elevated foot pressure through the plexiglass step is feasible and worth investigation as a clinical diagnostic tool.

BIOGRAPHY OF THE AUTHOR

Christian Crane was born in Houlton, Maine on February 14th, 1997. He was raised in Linneus, Maine and graduated from Houlton High School in 2015. He attended the University of Maine and graduated in 2021 with a Bachelors degree in Chemical Engineering and minor in Pre-Medical Studies. He transitioned to Biomedical Engineering due to his passion for medicine and interest in research. He began his graduate career in Biomedical Engineering in fall 2021 at University of Maine. His research into diabetic neuropathy detection was born from witnessing the resulting effects of this phenomenon and familial connections to diabetes. Christian is a candidate for the Master of Science degree in Biomedical Engineering from the University of Maine in May 2023.